# We are IntechOpen, the world's leading publisher of Open Access books
# Built by scientists, for scientists

## 6,900
Open access books available

## 185,000
International authors and editors

## 200M
Downloads

## 154
Countries delivered to

Our authors are among the
## TOP 1%
most cited scientists

## 12.2%
Contributors from top 500 universities

**BOOK CITATION INDEX**
CLARIVATE ANALYTICS
INDEXED

**WEB OF SCIENCE**™

Selection of our books indexed in the Book Citation Index
in Web of Science™ Core Collection (BKCI)

## Interested in publishing with us?
## Contact book.department@intechopen.com

Numbers displayed above are based on latest data collected.
For more information visit www.intechopen.com

# Generation and Propagation of Tsunami by a Moving Realistic Curvilinear Slide Shape with Variable Velocitie

Khaled T. Ramadan

Additional information is available at the end of the chapter

## 1. Introduction

Tsunamis are surface water waves caused by the impulsive perturbation of the sea. Apart from co-seismic sea bottom displacement due to earthquakes, sub-aerial and submarine landslides can also produce localized tsunamis with large and complex wave run-up especially along the coasts of narrow bays and fjords. In recent years, significant advances have been made in developing mathematical models to describe the entire process of generation, propagation and run-up of a tsunami event generated by seismic seafloor deformation [1-3].

The case of particular interest in this chapter is the mechanism of generation of tsunamis by submarine landslides. When a submarine landslide occurs, the ocean-bottom morphology may be significantly altered, in turn displacing the overlying water. Waves are then generated as water gets pulled down to fill the area vacated by the landslide and to a lesser extent, by the force of the sliding mass. Submarine slides can generate large tsunami, and usually result in more localized effects than tsunami caused by earthquakes [4]. Determination of volume, deceleration, velocity and rise time of the slide motion make modeling of tsunamis by submarine slides and slumps more complicated than simulation of seismic-generated tsunami.

Constant velocity implies that the slide starts and stops impulsively, i.e. the deceleration is infinite both initially and finally. Clearly, this is not true for real slides, and a more complex shape of the generated wave is expected [5].

In this chapter, we concern about the tsunami amplitudes predicted in the near-field caused by varying velocity of a two-dimensional realistic curvilinear slide model. The curvilinear

tsunami source model we considered based on available geological, seismological, and tsunami elevation. The aim of this chapter is to determine how near-field tsunami amplitudes change according to variable velocities of submarine slide. We discuss the nature and the extent of variations in the peak tsunami waveforms caused by time variations of the frontal velocity and the deceleration for the two-dimensional curvilinear block slide model and compares the results with those for the slide moving with constant velocity. It will show how the changes in the slide velocity as function in time acts to reduce wave focusing. Numerical results are presented for the normalized peak amplitude as a function of the propagation length of the slump and the slide, the water depth, the time variation of moving velocity and deceleration of the block slide. The problem is solved using linearized shallow-water theory for constant water depth by transform methods (Laplace in time and Fourier in space), with the forward and inverse Laplace transforms computed analytically, and the inverse Fourier transform computed numerically by the inverse Fast Fourier transform (IFFT).

## 2. Mathematical formulation of the problem

Consider a three dimensional fluid domain D as shown in Figure 1. It is supposed to represent the ocean above the fault area. It is bounded above by the free surface of the ocean $z = \eta(x, y, t)$ and below by the rigid ocean floor $z = -H(x, y) + \zeta(x, y, t)$, where $\eta(x, y, t)$ is the free surface elevation, $H(x, y)$ is the water depth and $\zeta(x, y, t)$ is the sea floor displacement function. The domain D is unbounded in the horizontal directions x and y, and can be written as $D = R^2 \times [(-H(x, y) + \zeta(x, y, t)), \eta(x, y, t)]$. For simplicity, $H(x, y)$ is assumed to be a constant. Before the earthquake, the fluid is assumed to be at rest, thus the free surface and the solid boundary are defined by $z = 0$ and $z = -H$, respectively. Mathematically, these conditions can be written in the form of initial conditions: $\eta(x, y, 0) = \zeta(x, y, 0) = 0$. At time $t > 0$ the bottom boundary moves in a prescribed manner which is given by $z = -H + \zeta(x, y, t)$. The resulting deformation of the free surface $z = \eta(x, y, t)$ is to be found as part of the solution. It is assumed that the fluid is incompressible and the flow is irrotational. The former implies the existence of a velocity potential $\phi(x, y, z, t)$ which fully describes the flow and the physical process. By definition of $\phi$, the fluid velocity vector can be expressed as $\vec{u} = \nabla \phi$. Thus, the potential flow $\phi(x, y, z, t)$ must satisfy the Laplace's equation

$$\nabla^2 \phi(x, y, z, t) = 0 \text{ where } (x, y, z) \in R^2 \times [-H, 0], \tag{1}$$

subjected to the following linearized kinematic and dynamic boundary conditions on the free surface and the solid boundary, respectively
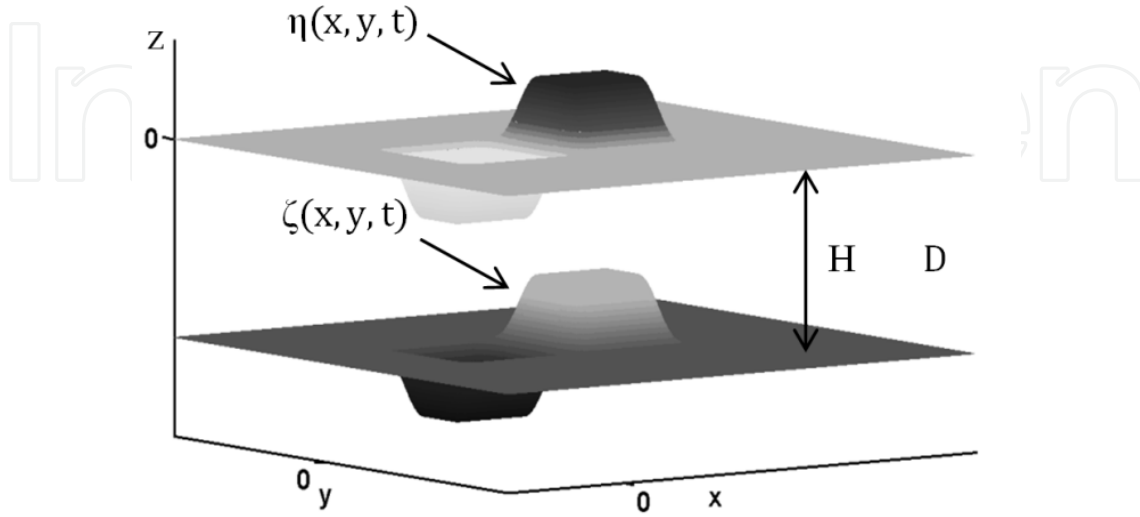
$$\phi_z = \eta_t \text{ on } z = 0, \tag{2}$$

$$\phi_z = \zeta_t \text{ on } z = -H, \tag{3}$$

$$\phi_t + g\eta = 0 \text{ on } z = 0, \tag{4}$$

with the initial conditions given by

$$\phi(x, y, z, 0) = \eta(x, y, 0) = \zeta(x, y, 0) = 0. \tag{5}$$

So, the linearized shallow water solution can be obtained by the Fourier-Laplace transforms.



**Figure 1.** Fluid domain and coordinate system for a very rapid movement of the assumed source model.

## 2.1. Solution of the problem

Our interest is focused on the resulting uplift of the free surface elevation $\eta(x, y, t)$. An analytical analyses is to examine and illustrate the generation and propagation of a tsunami for a given bed profile $\zeta(x, y, t)$. Mathematical modeling of waves generated by vertical and lateral displacements of ocean bottom using the combined Fourier–Laplace transform of the Laplace equation analytically is the simplest way of studying tsunami development. Equations (1)–(4) can be solved by using the method of integral transforms. We apply the Fourier transform in (x, y)

$$\mathfrak{F}[f] = F(k_1, k_2) = \int_{R^2} f(x, y) e^{-i(x k_1 + y k_2)} \, dx \, dy,$$

with its inverse transform

$$\mathfrak{F}^{-1}[F] = f(x, y) = \frac{1}{(2\pi)^2} \int_{R^2} F(k_1, k_2) \, e^{i(x k_1 + y k_2)} \, dk_1 \, dk_2 ,$$

and the Laplace transform in time t,

$$\pounds [g] = G(s) = \int_0^\infty g(t) e^{-s t} \, dt$$

For the combined Fourier-Laplace transforms, the following notation is introduced:

$$\mathfrak{F}(\pounds(f(x, y, t))) = \bar{F}(k_1, k_2, s) = \int_{R^2} e^{-i(x k_1 + y k_2)} \left[ \int_0^\infty f(x, y, t) \, e^{-s t} \, dt \right] dx \, dy$$

Combining (2) and (4) yields the single free-surface condition

$$\phi_{tt}(x, y, 0, t) + g\phi_z(x, y, 0, t) = 0 \tag{6}$$

and the bottom condition (3) will be

$$\phi_z(x, y, -H, t) = \zeta_t(x, y, t) \tag{7}$$

The solution of the Laplace equation (1) which satisfies the boundary conditions (6) & (7) can be obtained by using the Fourier-Laplace transforms method.

First, by applying the transforms method to the Laplace equation (1), gives

$$\mathfrak{F}\left\{ \pounds \left( \frac{\partial^2 \phi}{\partial x^2} \right) \right\} + \mathfrak{F}\left\{ \pounds \left( \frac{\partial^2 \phi}{\partial y^2} \right) \right\} + \mathfrak{F}\left\{ \pounds \left( \frac{\partial^2 \phi}{\partial z^2} \right) \right\} = 0 \tag{8}$$

By using the property $\left\{ \frac{d^n f}{dx^n} \right\} = (ik)^n \bar{F}(k)$, Equation (8) will be

$$\bar{\phi}_{zz}(k_1, k_2, z, s) - \left( k_1^2 + k_2^2 \right) \bar{\phi}(k_1, k_2, z, s) = 0 \tag{9}$$

Second, by applying the transforms method to the boundary conditions (6) & (7) and the initial conditions (5), yields

$$s^2 \bar{\phi}(k_1, k_2, 0, s) + g\, \bar{\phi}_z(k_1, k_2, 0, s) = 0, \tag{10}$$

and

$$\bar{\phi}_z(k_1, k_2, -h, s) = s\bar{\zeta}(k_1, k_2, s) \tag{11}$$

The transformed free-surface elevation can be obtained from (4) as

$$\bar{\eta}(k_1, k_2, s) = -\frac{s}{g}\, \bar{\phi}(k_1, k_2, 0, s) \tag{12}$$

The general solution of (9) will be

$$\bar{\phi}(k_1, k_2, z, s) = A(k_1, k_2, s)\cosh(kz) + B(k_1, k_2, s)\sinh(kz), \tag{13}$$

where $k = \sqrt{k_1^2 + k_2^2}$. The functions $A(k_1, k_2, s)$ and $B(k_1, k_2, s)$ can be found from the boundary conditions (10) & (11) as follows

For the bottom condition (at $z = -h$):

$$\frac{\partial \bar{\phi}(k_1, k_2, -h, s)}{\partial z} = -Ak\sinh(kh) + Bk\cosh(kh) \tag{14}$$

Substituting from (14) into (11), yields

$$-Ak\sinh(kh) + Bk\cosh(kh) = s\bar{\zeta}(k_1, k_2, s) \tag{15}$$

For the free surface condition (at $z = 0$):

$$\frac{\partial \overline{\phi}(k_1,k_2,0,s)}{\partial z} = Bk \text{ and } \overline{\phi}(k_1,k_2,0,s) = A \tag{16}$$

Substituting from (16) into (10), gives

$$A = \frac{-g\,k}{s^2} B \tag{17}$$

Using (17), Equation (15) can be written as

$$Bk\cosh(kh)\left[1 + \frac{gk}{s^2}\tanh(kh)\right] = s\,\overline{\zeta}(k_1,k_2,s). \tag{18}$$

From which,

$$A(k_1,k_2,s) = -\frac{g\,s\,\overline{\zeta}(k_1,k_2,s)}{\cosh(kh)[s^2+g\,k\,\tanh(kh)]}, B(k_1,k_2,s) = \frac{s^3\,\overline{\zeta}(k_1,k_2,s)}{k\cosh(kh)[s^2+g\,k\,\tanh(kh)]}.$$

Substituting the expressions for the functions $A(k_1,k_2,s)$ and $B(k_1,k_2,s)$ in (13) yields,

$$\overline{\phi}(k_1,k_2,z,s) = -\frac{g\,s\,\overline{\zeta}(k_1,k_2,s)}{\cosh(kh)(s^2+\omega^2)}\left(\cosh(kz) - \frac{s^2}{g\,k}\sinh(kz)\right), \tag{19}$$

where $\omega = \sqrt{g\,k\,\tanh(kh)}$ is the circular frequency of the wave motion.

The free surface elevation $\overline{\eta}(k_1,k_2,s)$ can be obtained from (12) as

$$\overline{\eta}(k_1,k_2,s) = \frac{s^2\,\overline{\zeta}(k_1,k_2,s)}{\cosh(kh)(s^2+\omega^2)} \tag{20}$$

A solution for $\eta(x,y,t)$ can be evaluated for specified by computing approximately its transform $\overline{\zeta}(k_1,k_2,s)$ then substituting it into (20) and inverting $\overline{\eta}(k_1,k_2,s)$ to obtain $\eta(x,y,t)$. We concern to evaluate $\eta(x,y,t)$ by transforming analytically the assumed source model then inverting the Laplace transform of $\overline{\eta}(k_1,k_2,s)$ to obtain $\overline{\eta}(k_1,k_2,t)$ which is further converted to $\eta(x,y,t)$ by using double inverse Fourier Transform.

The circular frequency $\omega$ describes the dispersion relation of tsunamis and implies phase velocity $c_p = \frac{\omega}{k}$ and group velocity $c_g = \frac{d\omega}{dk}$. Hence, $c_p = \sqrt{\frac{g\tanh(kH)}{k}}$, and $c_g = \frac{1}{2}c_p\left(1 + \frac{2kH}{\sinh(2kH)}\right)$. Since, $k = \frac{2\pi}{\lambda}$, hence as $kH \to 0$, both $c_p \to \sqrt{gH}$ and $c_g \to \sqrt{gH}$, which implies that the tsunami velocity $v_t = \sqrt{gH}$ for wavelengths $\lambda$ long compared to the water depth H. The above linearized solution is known as the shallow water solution.

We considered three stages for the mechanism of the tsunami generation caused by submarine gravity mass flows, initiated by a rapid curvilinear down and uplift faulting with rise time $0 \leq t \leq t_1$, then propagating unilaterally in the positive $x-$ direction with time $t_1 \leq t \leq t^*$, to a length L both with finite velocity v to produce a depletion and an accumulation zones. The last stage represented by the time variation in the velocity of the accumulation slide (block slide) moving in the $x-$ direction with time $t^* \leq t \leq t_{max}$ and deceleration $\alpha$, where $t_{max}$ is the maximum time that the slide takes to stop with minimum deceleration $\alpha_{min}$. In the $y-$direction, the models propagate instantaneously. The set of physical parameters used in the problem are given in Table 1.

| PARAMETERS | FIRST STAGE | SECOND STAGE |
|---|---|---|
| Source width, W , km | 100 | 100 |
| Whole width in 1st Stage and Propagation length in 2nd Stage, km | W' = 100 | L = 150 |
| Water depth (uniform), H , km | 2 | 2 |
| Acceleration due to gravity, g, km/sec² | 0.0098 | 0.0098 |
| Tsunami velocity, $v_t = \sqrt{gH}$ , km/sec | 0.14 | 0.14 |
| Moving velocity, v, km/sec , to obtain maximum surface amplitude | 0.14 | 0.14 |
| Duration of the source process, t , min | $t_1 = \frac{50}{v}$ =5.95 | $t^* = \frac{200}{v}$=23.8 |

**Table 1.** Parameters used in the analytical solution of the problem.

The first and second stages of the bed motion are shown in Figure 2 and Figure 3, respectively, and given by:

a.   First stage: Curvilinear down and uplift faulting for $0 \le t \le t_1$

where for $x \in [-50, 50]$

$$\zeta_{down}(x,y,t) = \begin{cases} -\zeta_0 \frac{vt}{2S} \left(1+\cos\frac{\pi}{50}x\right)\left[1-\cos\frac{\pi}{100}(y+150)\right], & -150 \le y \le -50, \\ -\zeta_0 \frac{vt}{S} \left(1+\cos\frac{\pi}{50}x\right) & , -50 \le y \le 50, \\ -\zeta_0 \frac{vt}{2S} \left(1+\cos\frac{\pi}{50}x\right)\left[1+\cos\frac{\pi}{100}(y-50)\right], & 50 \le y \le 150. \end{cases} \qquad (21)$$

and for $x \in [200, 300]$

$$\zeta_{up}(x,y,t) = \begin{cases} \zeta_0 \frac{vt}{2S} \left(1-\cos\frac{\pi}{50}(x-200)\right)\left[1-\cos\frac{\pi}{100}(y+150)\right], & -150 \le y \le -50, \\ \zeta_0 \frac{vt}{S} \left(1-\cos\frac{\pi}{50}(x-200)\right) & , -50 \le y \le 50, \\ \zeta_0 \frac{vt}{2S} \left(1-\cos\frac{\pi}{50}(x-200)\right)\left[1+\cos\frac{\pi}{100}(y-50)\right], & 50 \le y \le 150. \end{cases} \qquad (22)$$

For these displacements, the bed rises during $0 \le t \le t_1$ to a maximum displacement $\zeta_0$ such that the volume of soil in the uplift increases linear with time and vise verse in the down faulting.

For $t \ge t_1$ the soil further propagates unilaterally in the positive x- direction with velocity v till it reaches the characteristic length L = 150 km at t = t*= 200/v .

(a)



(b)
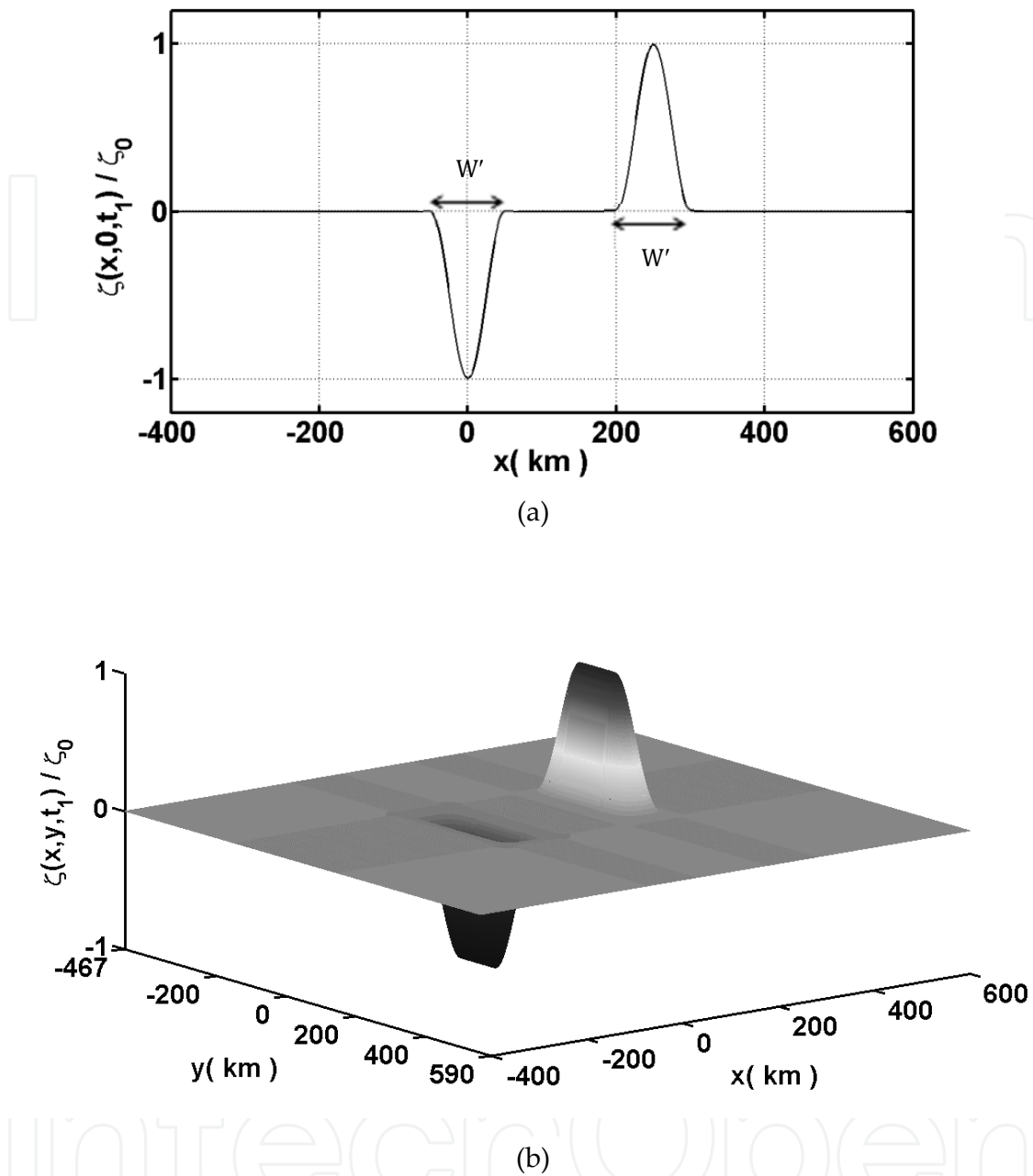
(a) Side view along the axis of symmetry at $y = 0$ (b) Three- dimensional view.

**Figure 2.** Normalized bed deformation represented by a rapid curvilinear down and uplift faulting at the end of stage one $(t_1 = \frac{50}{v})$

b.   Second stage: Curvilinear down and uphill slip-fault (slump and the slide) for $t_1 \leq t \leq t^*$

$$\zeta_{down}(x, y, t) = \zeta_{1down}(x, y, t) + \zeta_{2down}(x, y, t) + \zeta_{3down}(x, y, t), \tag{23}$$

where for $y \in [-150, -50]$

$$\zeta_{1\text{down}}(x,y,t) = \begin{cases} -\dfrac{\zeta_0}{4}\left(1+\cos\dfrac{\pi}{50}x\right)\left[1-\cos\dfrac{\pi}{100}\left(y+150\right)\right], & -50 \leq x \leq 0, \\[3mm] -\dfrac{\zeta_0}{2}\left[1-\cos\dfrac{\pi}{100}\left(y+150\right)\right], & 0 \leq x \leq (t\text{-}t_1)\,v, \\[3mm] -\dfrac{\zeta_0}{4}\left[1+\cos\dfrac{\pi}{50}\left(x-\left(t\text{-}t_1\right)v\right)\right]\left[1-\cos\dfrac{\pi}{100}\left(y+150\right)\right], & \left(t\text{-}t_1\right)v \leq x \leq \left(t\text{-}t_1\right)v+50, \end{cases}$$

and for $y \in [-50, 50]$

$$\zeta_{2\text{down}}(x,y,t) = \begin{cases} -\dfrac{\zeta_0}{2}\left(1+\cos\dfrac{\pi}{50}x\right), & -50 \leq x \leq 0, \\[3mm] -\zeta_0, \ 0 \leq x \leq \left(t\text{-}t_1\right)v, \\[3mm] -\dfrac{\zeta_0}{2}\left[1+\cos\dfrac{\pi}{50}\left(x-\left(t\text{-}t_1\right)v\right)\right], & \left(t\text{-}t_1\right)v \leq x \leq \left(t\text{-}t_1\right)v+50, \end{cases}$$

and for $y \in [50, 150]$

$$\zeta_{3\text{down}}(x,y,t) = \begin{cases} -\dfrac{\zeta_0}{4}\left(1+\cos\dfrac{\pi}{50}x\right)\left[1+\cos\dfrac{\pi}{100}\left(y-50\right)\right], & -50 \leq x \leq 0, \\[3mm] -\dfrac{\zeta_0}{2}\left[1+\cos\dfrac{\pi}{100}\left(y-50\right)\right], & 0 \leq x \leq (t\text{-}t_1)\,v, \\[3mm] -\dfrac{\zeta_0}{4}\left[1+\cos\dfrac{\pi}{50}\left(x-(t\text{-}t_1)\,v\right)\right]\left[1+\cos\dfrac{\pi}{100}\left(y-50\right)\right], & (t\text{-}t_1)\,v \leq x \leq (t\text{-}t_1)\,v+50, \end{cases}$$

$$\zeta_{up}(x,y,t) = \zeta_{1up}(x,y,t) + \zeta_{2up}(x,y,t) + \zeta_{3up}(x,y,t), \tag{24}$$

where for $y \in [-150, -50]$

$$\zeta_{1up}(x,y,t) = \begin{cases} \dfrac{\zeta_0}{4}\left(1-\cos\dfrac{\pi}{50}(x-200)\right)\left[1-\cos\dfrac{\pi}{100}\left(y+150\right)\right] & 200 \leq x \leq 250, \\[3mm] \dfrac{\zeta_0}{2}\left[1-\cos\dfrac{\pi}{100}\left(y+150\right)\right], & 250 \leq x \leq 250+(t\text{-}t_1)\,v, \\[3mm] \dfrac{\zeta_0}{4}\left[1+\cos\dfrac{\pi}{50}\left(x-\left(250+\left(t\text{-}t_1\right)v\right)\right)\right]\left[1-\cos\dfrac{\pi}{100}\left(y+150\right)\right] & 250+\left(t\text{-}t_1\right)v \leq x \leq 300+\left(t\text{-}t_1\right)v, \end{cases}$$

and for $y \in [-50, 50]$

$$\zeta_{2up}(x,y,t) = \begin{cases} \dfrac{\zeta_0}{2}\left(1-\cos\dfrac{\pi}{50}(x-200)\right), & 200 \leq x \leq 250 \\[3mm] \zeta_0, \ 250 \leq x \leq 250+\left(t\text{-}t_1\right)v, \\[3mm] \dfrac{\zeta_0}{2}\left[1+\cos\dfrac{\pi}{50}\left(x-\left(250+\left(t\text{-}t_1\right)v\right)\right)\right], & 250+\left(t\text{-}t_1\right)v \leq x \leq 300+\left(t\text{-}t_1\right)v, \end{cases}$$

and for $y \in [\, 50, 150]$

$\zeta_{3up}(x, y, t) =$

$$
\begin{cases}
\dfrac{\zeta_0}{4}\left(1 - \cos\dfrac{\pi}{50}(x\text{-}200)\right)\left[\,1 + \cos\dfrac{\pi}{100}(\,y\text{ -}50\,)\,\right] , & 200 \le x \le 250 , \\[3mm]
\dfrac{\zeta_0}{2}\left[\,1 + \cos\dfrac{\pi}{100}(\,y\text{ -}50\,)\,\right] , & 250 \le x \le 250 + (t\text{-}t_1)\,v , \\[3mm]
\dfrac{\zeta_0}{4}\left[\,1 + \cos\dfrac{\pi}{50}\bigl(x\text{-}(250 + (t\text{ -}t_1)\,v)\bigr)\right]\left[\,1 + \cos\dfrac{\pi}{100}(\,y\text{ -}50\,)\,\right] , & 250 + (t\text{-}t_1)\,v \le x \le 300 + (t\text{-}t_1)
\end{cases}
$$

The kinematic realistic tsunami source model shown in Figure 3 is initiated by a rapid curvilinear down and uplift faulting (First stage) which then spreads unilaterally with constant velocity v causing a depletion and accumulation zone. The final down lift of the depression zone and final uplift of the accumulation zone are assumed to have the same amplitude $\zeta_0$. We assume the spreading velocity v of the slump and the slide deformation in Figure 3 the same as the tsunami wave velocity $v_t = \sqrt{gH}$ as the largest amplification of the tsunami amplitude occurs when $v = v_t$ due to wave focusing . The slide and the slump are assumed to have constant width W.

The spreading is unilateral in the x-direction as shown in Figure 3. The vertical displacement, $\zeta_0$, is negative (downwards) in zones of depletion, and positive (upwards) in zones of accumulation. All cases are characterized by sliding motion in one direction, without loss of generality coinciding with the x-axis, and tsunami propagating in the x-y plane.

Figure 4 shows vertical cross-sections (through y = 0) of the mathematical models of the stationary submarine slump and the moving slide and their schematic representation of the physical process that we considered in this study, as those evolve for time $t \ge t^*$ . The block slide starts moving in the positive x-direction at time $t = t^*$ and stops moving at distance $L' = 150$ km while the downhill slide becomes stationary. We discuss the tsunami generation for two cases of the movement of the block slide. First, the limiting case in which the block slide moves with constant velocity v and stops after distance L′ with infinite deceleration (sudden stop) at time $t_{min} = t^* + L'/v$.

Second, the general case in which the block slide moves in time $t_2 \ge t^*$ with constant velocity and then with constant deceleration such that it stop softly after traveling the same distance L′ in time $t_3$ which depends on the deceleration α and the choice of time $t_2$.

The velocity v(t) in this case can be defined as

$$
v(t) = \begin{cases} v & t^* \le t \le t_2 \\ v - (t - t_2)\alpha , & t_2 \le t \le t_3 \end{cases} , \tag{25}
$$

where $v = v_t = 0.14$ km/sec and α is the deceleration of the moving block slide. We need to determine the time $t_3$ that the slide takes to reach the final distance L′ and the corresponding deceleration α . This can be done by using the following steps:

(a)



(b)
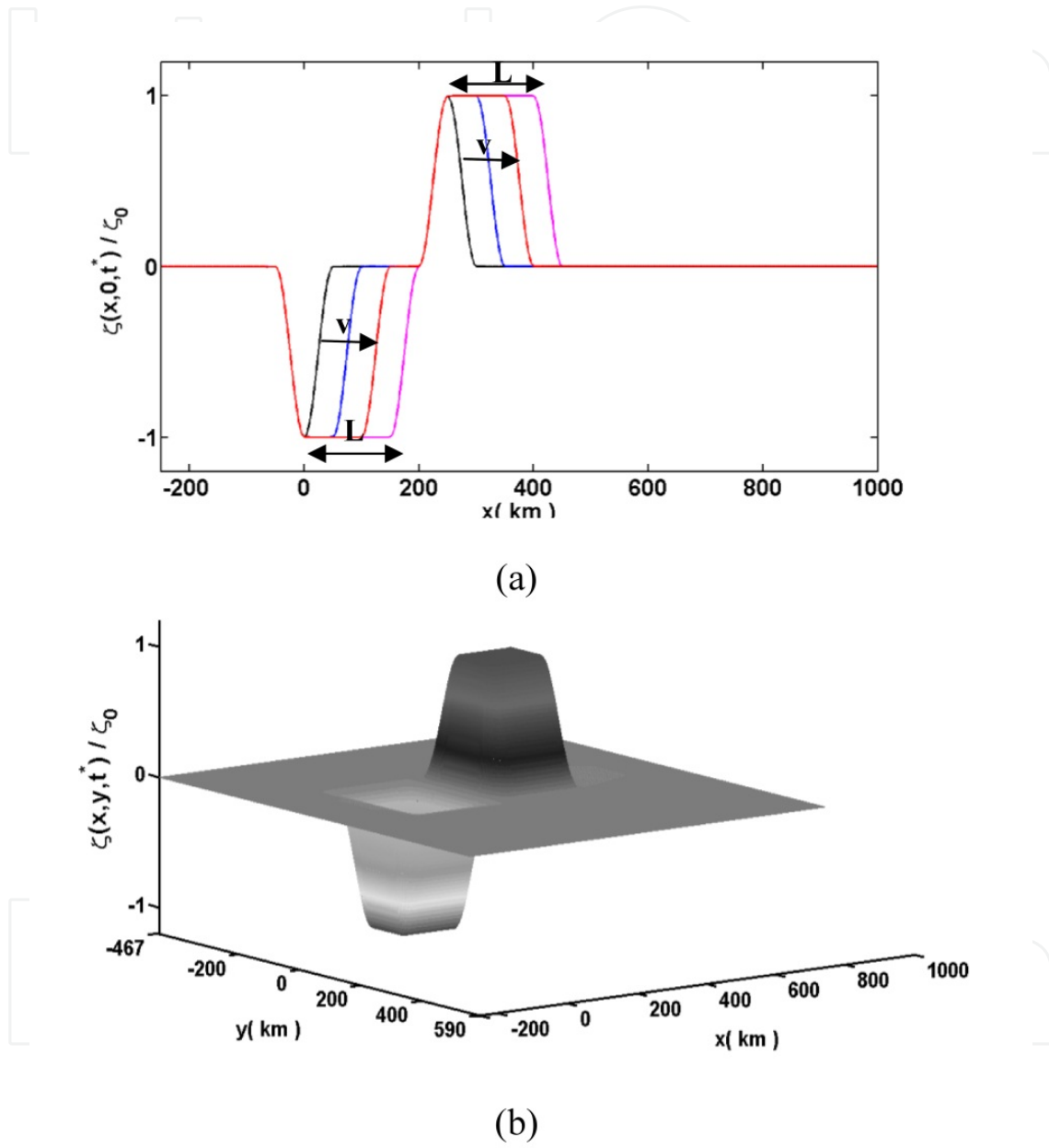
**Figure 3.** Normalized Bed deformation model represented by the accumulation and depletion zones at the end of stage two ($t^* = \frac{200}{v}$) (a) Side view along the axis of symmetry at $y = 0$ b) Three-dimensional view.
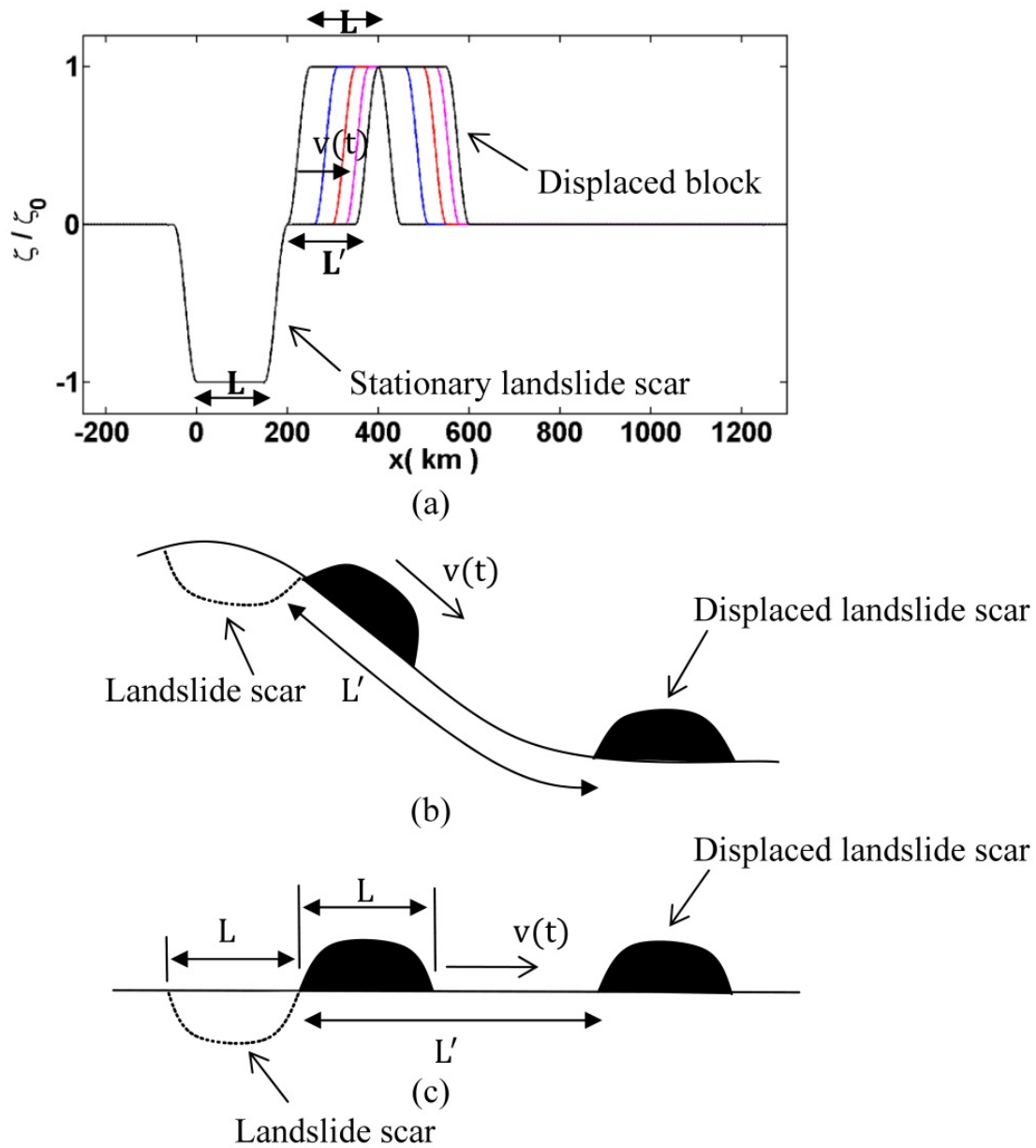
(a)    Case 1: Mathematical model of the stationary slump and the moving submarine slide.

(b)    Case 2: Physical process of the displaced block moving with a variable slide velocity v(t).

(c)    Case 3: Schematic representation of the used model.

**Figure 4.** A schematic representation of a landslide (bottom) travelling a significant distance L downhill creating a ''scar'' and a moving uphill displaced block slide stopping at the characteristic length L′.

1.  Choosing time $t_2$ as $t^* \leq t_2 \leq t^* + (L'/v)$ in which the slide moves with constant velocity $v$ where $t^* = t_1 + L/v$ and $t_1 = 50/v$.
2.  Getting the corresponding distance $L^* = (t_2 - t^*)v$.
3.  Evaluating the remaining distance $L^{**} = L' - (t_2 - t^*)v$.

Substituting $L^{**}$ in the equation

$$L^{**} = (t_3 - t_2)v - \frac{1}{2}\alpha(t_3 - t_2)^2 \qquad (26)$$

When the block slide stops moving, then

$$v(t) = v - (t_3 - t_2)\alpha = 0 \qquad (27)$$

Eliminating $\alpha$ from equations (7.12) and (7.13), we get relation between $t_3$ and $t_2$ which further substituting in equation (7.13), we obtain the deceleration $\alpha$.

For $t_2 \leq t \leq t_3$, the block slide moves with velocity $v(t) = v - (t - t_2)\alpha$. Table 2 represents different values of $t_2$ and the corresponding calculated value of $t_3$ and $\alpha$.

| TIME $t_2$ (MIN) | TIME $t_3$ (MIN) | DECELERATION $\alpha$ (km/sec$^2$) |
|---|---|---|
| $t^* = 23.80$ | 59.51 | $6.53 \times 10^{-5}$ |
| $t^* + 0.1(L'/v) = 25.58$ | 57.72 | $7.25 \times 10^{-5}$ |
| $t^* + 0.2(L'/v) = 27.37$ | 55.95 | $8.16 \times 10^{-5}$ |
| $t^* + 0.3(L'/v) = 29.37$ | 54.15 | $9.33 \times 10^{-5}$ |
| $t^* + 0.4(L'/v) = 30.94$ | 52.36 | $1.08 \times 10^{-4}$ |
| $t^* + 0.5(L'/v) = 32.72$ | 50.57 | $1.30 \times 10^{-4}$ |
| $t^* + 0.6(L'/v) = 34.51$ | 48.79 | $1.63 \times 10^{-4}$ |
| $t^* + 0.7(L'/v) = 36.30$ | 47.01 | $2.17 \times 10^{-4}$ |
| $t^* + 0.8(L'/v) = 38.08$ | 45.22 | $3.26 \times 10^{-4}$ |
| $t^* + 0.9(L'/v) = 39.87$ | 43.44 | $6.53 \times 10^{-4}$ |
| $t^* + (L'/v) = 41.65$ | 41.65 | Infinity |

**Table 2.** Values of $t_2$ and the corresponding calculated values of $t_3$ and .

Figure 5 illustrates the position of the slides in the third stage for different choice of deceleration α. In this stage, $\alpha_{min}$ is the minimum deceleration required such that the slide stops after traveling distance $L'$. In this case $t_2 = t^*$ and $t_3 = t_{max} = t^* + (2L'/v) = 59.51$ min. For any other $\alpha > \alpha_{min}$, the slide moves with constant velocity with time $t^* \leq t \leq t_2$ and with deceleration α until it stops at time $t_3$ which is less than $t_{max}$.

So, the stationary landslide scar for $t^* \leq t$ and the movable block slide with variable velocity $v(t)$ for $t^* \leq t_2 \leq t^* + (L'/v)$ and $t^* + (L'/v) \leq t_3 \leq t^* + (2L'/v)$ can be expressed respectively as

$$\zeta_{stat.landslide}(x, y, t^*) = \zeta_1(x, y, t^*) + \zeta_2(x, y, t^*) + \zeta_3(x, y, t^*), \qquad (28)$$
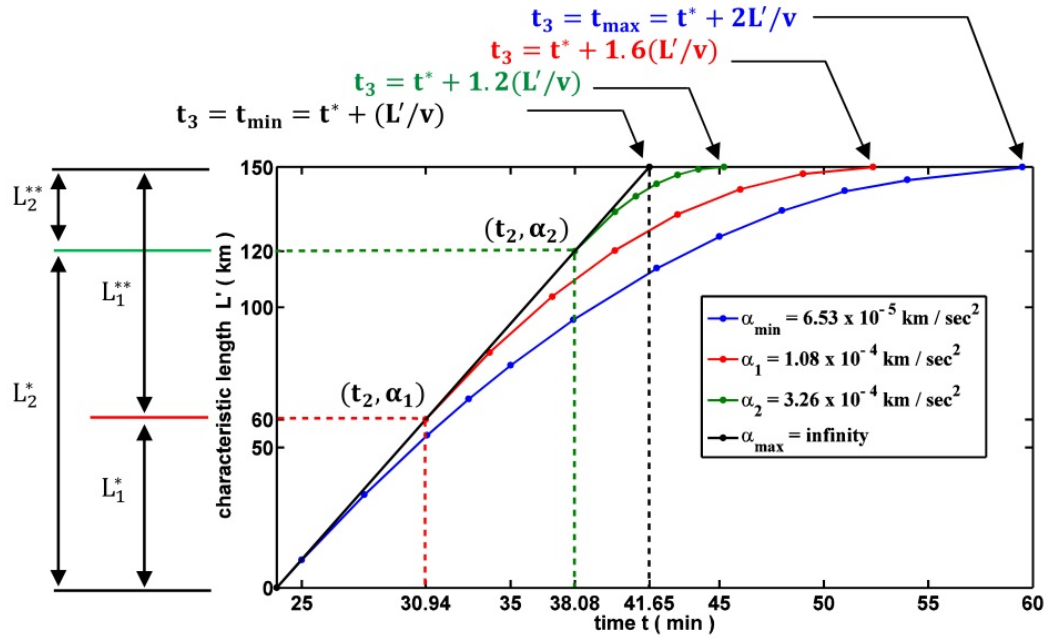
**Figure 5.** Slide block position against the instants of times $t^* \leq t_2 \leq t^* + (L'/v)$ and $t_{min} \leq t_3 \leq t_{max}$.

$$\zeta_{\text{block slide}}(x, y, t) = \zeta_1(x, y, t) + \zeta_2(x, y, t) + \zeta_3(x, y, t), \qquad (29)$$

$\zeta_{\text{stat.landslide}}(x, y, t^*)$ is the same as (23) except the time parameter t will be substituted by $t^*$.

For $\zeta_{\text{block slide}}(x, y, t)$, let $S = \begin{cases} (t - t^*)v \text{ for } t^* \leq t \leq t_2, \\ (t - t^*)v - \frac{1}{2}\alpha(t - t_2)^2 \text{ for } t_2 \leq t \leq t_3, \end{cases}$ be

the distance the slide moves during stage three, hence

for $y \in [-150, -50]$

$$\zeta_1(x, y, t) = \begin{cases} \frac{\zeta_0}{4}\left(1 - \cos\frac{\pi}{50}(x-(200+S))\right)\left[1-\cos\frac{\pi}{100}(y+150)\right], 200+S \leq x \leq 250+S, \\ \frac{\zeta_0}{2}\left[1- \cos\frac{\pi}{100}(y+150)\right], 250+S \leq x \leq 250+S+L, \\ \frac{\zeta_0}{4}\left[1+\cos\frac{\pi}{50}(x-(250+S+L))\right]\left[1-\cos\frac{\pi}{100}(y+150)\right], 250+S+L \leq x \leq 300+S+L, \end{cases}$$

and for $y \in [-50, 50]$

$$\zeta_2(x, y, t) = \begin{cases} \frac{\zeta_0}{2}\left(1 - \cos\frac{\pi}{50}(x-(200+S))\right), 200+S \leq x \leq 250+S, \\ \zeta_0, 250+S \leq x \leq 250+S+L, \\ \frac{\zeta_0}{2}\left[1+\cos\frac{\pi}{50}(x-(250+S+L))\right], 250+S+L \leq x \leq 300+S+L, \end{cases}$$

and for $y \in [50, 150]$

$$\zeta_3(x,y,t_2,t_3) = \begin{cases} \frac{\zeta_0}{4}\left(1 - \cos\frac{\pi}{50}(x-(200+S))\right)\left[1+\cos\frac{\pi}{100}\left(y-50\right)\right], & 200+S \le x \le 250+S, \\[2mm] \frac{\zeta_0}{2}\left[1+\cos\frac{\pi}{100}\left(y-50\right)\right], & 250+S \le x \le 250+S+L, \\[2mm] \frac{\zeta_0}{4}\left[1+\cos\frac{\pi}{50}\left(x-(250+S+L)\right)\right]\left[1+\cos\frac{\pi}{100}\left(y-50\right)\right], & 250+S+L \le x \le 300+S+L, \end{cases}$$

Laplace and Fourier transforms can now applied to the bed motion described by Equations (21)-(24) and Equations (28) & (29). First, beginning with the curvilinear down and uplift faulting (21) and (22) for $0 \le t \le t_1$ where $t_1 = \frac{50}{v}$, and

$$\mathfrak{F}(\pounds(\zeta(x,y,t)) = \bar{\zeta}(k_1,k_2,s) = \int_{-\infty}^{\infty} e^{-i(xk_1+yk_2)}\left[\int_{0}^{\infty}\zeta(x,y,t)\,e^{-st}\,dt\right]dx\,dy. \qquad (30)$$

The limits of the above integration are apparent from Equations (21) & (22) and are done as follows:

$$\zeta_{\text{down}}(k_1,k_2,s) =$$

$$\int_{-150}^{-50}\frac{1}{2}\left[1-\cos\frac{\pi}{100}(y+150)\right]e^{-ik_2y}dy\left[\int_{-50}^{50}\left(1+\cos\frac{\pi}{50}x\right)e^{-ik_1x}dx\int_{0}^{\infty}-\zeta_0\frac{vt}{2S}e^{-st}dt\right]$$

$$+\int_{-50}^{50}e^{-ik_2y}\,dy\left[\int_{-50}^{50}\left(1+\cos\frac{\pi}{50}x\right)e^{-ik_1x}dx\int_{0}^{\infty}-\zeta_0\frac{vt}{S}e^{-st}dt\right]$$

$$+\int_{50}^{150}\frac{1}{2}\left[1+\cos\frac{\pi}{100}\left(y-50\right)\right]e^{-ik_2y}dy\left[\int_{-50}^{50}\left(1+\cos\frac{\pi}{50}x\right)e^{-ik_1x}dx\int_{0}^{\infty}-\zeta_0\frac{vt}{2S}e^{-st}dt\right],$$

$$\zeta_{\text{up}}(k_1,k_2,s) =$$

$$\int_{-150}^{-50}\frac{1}{2}\left[1-\cos\frac{\pi}{100}(y+150)\right]e^{-ik_2y}dy\left[\int_{200}^{300}\left(1-\cos\frac{\pi}{50}(x-200)\right)e^{-ik_1x}dx\int_{0}^{\infty}\zeta_0\frac{vt}{2S}e^{-st}dt\right]$$

$$+\int_{-50}^{50}e^{-ik_2y}\,dy\left[\int_{200}^{300}\left(1-\cos\frac{\pi}{50}(x-200)\right)e^{-ik_1x}dx\int_{0}^{\infty}\zeta_0\frac{vt}{S}e^{-st}dt\right]$$

$$+\int_{50}^{150}\frac{1}{2}\left[1+\cos\frac{\pi}{100}\left(y-50\right)\right]e^{-ik_2y}dy\left[\int_{-50}^{50}\left(1-\cos\frac{\pi}{50}(x-200)\right)e^{-ik_1x}dx\int_{0}^{\infty}\zeta_0\frac{vt}{2S}e^{-st}dt\right],$$

Substituting the results of the integration for $\zeta_{\text{down}}$ and $\zeta_{\text{up}}$ into (20), yields

$$\bar{\eta}(k_1,k_2,s) =$$

$$\frac{1}{\cosh(kH)(s^2+\omega^2)}\zeta_0\frac{v}{L}\frac{1}{2}\left[\begin{array}{l}\left[\frac{(e^{-i\,200\,k_1}-e^{-i\,300\,k_1})}{ik_1}-\frac{1}{1-\left(\frac{50}{\pi}k_1\right)^2}\left[ik_1\left(\frac{50}{\pi}\right)^2(e^{-i300k_1}-e^{i200k_1})\right]\right]- \\[4mm] \left[\frac{(e^{i\,50\,k_1}-e^{-i\,50\,k_1})}{ik_1}+\frac{1}{1-\left(\frac{50}{\pi}k_1\right)^2}\left[ik_1\left(\frac{50}{\pi}\right)^2(e^{-i50k_1}-e^{i50k_1})\right]\right]\end{array}\right] \times$$

$$\left[\begin{array}{l}\frac{(e^{i\,150\,k_2}-e^{i\,50\,k_2})}{i\,k_2}-\dfrac{1}{1-\left(\frac{100}{\pi}k_2\right)^2}\left[ik_2\left(\dfrac{100}{\pi}\right)^2(e^{i50k_2}+e^{i150k_2})\right]+\dfrac{4\sin(50k_2)}{k_2}+\\[4mm]\left[\frac{(e^{-i\,50\,k_2}-e^{-i\,150\,k_2})}{i\,k_2}+\dfrac{1}{1-\left(\frac{100}{\pi}k_2\right)^2}\left[ik_2\left(\dfrac{100}{\pi}\right)^2(e^{-i150k_2}+e^{-i50k_2})\right]\right]\end{array}\right].$$
(31)

The free surface elevation $\bar{\eta}(k_1,k_2,t)$ can be evaluated by using the inverse Laplace transforms of $\bar{\eta}(k_1,k_2,s)$ given by Equation (31) as follows:

First, recall that $\pounds^{-1}\left\{\dfrac{1}{s^2+\omega^2}\right\}=\dfrac{\sin\omega t}{\omega}$ hence $\bar{\eta}(k_1,k_2,t)$ becomes

$\bar{\eta}(k_1,k_2,t)=$

$$\dfrac{\sin\omega t}{\omega\cosh(kH)}\dfrac{\zeta_0\,v}{2L}\left[\begin{array}{l}\left[\dfrac{(e^{-i\,200\,k_1}-e^{-i\,300\,k_1})}{ik_1}-\dfrac{1}{1-\left(\frac{50}{\pi}k_1\right)^2}\left[ik_1\left(\dfrac{50}{\pi}\right)^2(e^{-i300k_1}-e^{i200k_1})\right]\right]-\\[6mm]\left[\dfrac{(e^{i\,50\,k_1}-e^{-i\,50\,k_1})}{ik_1}+\dfrac{1}{1-\left(\frac{50}{\pi}k_1\right)^2}\left[ik_1\left(\dfrac{50}{\pi}\right)^2(e^{-i50k_1}-e^{i50k_1})\right]\right]\end{array}\right]$$

$$\times\left[\begin{array}{l}\frac{(e^{i\,150\,k_2}-e^{i\,50\,k_2})}{i\,k_2}-\dfrac{1}{1-\left(\frac{100}{\pi}k_2\right)^2}\left[ik_2\left(\dfrac{100}{\pi}\right)^2(e^{i50k_2}+e^{i150k_2})\right]+\dfrac{4\sin(50k_2)}{k_2}+\\[4mm]\left[\frac{(e^{-i\,50\,k_2}-e^{-i\,150\,k_2})}{i\,k_2}+\dfrac{1}{1-\left(\frac{100}{\pi}k_2\right)^2}\left[ik_2\left(\dfrac{100}{\pi}\right)^2(e^{-i150k_2}+e^{-i50k_2})\right]\right]\end{array}\right].$$
(32)

In case for $t\geq t_1$, $\bar{\eta}(k_1,k_2,t)$ will have the same expression except in the convolution step, the integral

become $\int_{t-t_1}^{t}\cos\omega\tau\,d\tau=\dfrac{\sin\omega t}{\omega}-\dfrac{\sin\omega(t-t_1)}{\omega}$ instead of $\int_{0}^{t}\cos\omega\tau\,d\tau=\dfrac{\sin\omega t}{\omega}$.

Finally, $\eta(x,y,t)$ is evaluated using the double inverse Fourier transform of $\bar{\eta}(k_1,k_2,t)$

$$\eta(x,y,t)=\dfrac{1}{(2\pi)^2}\int_{-\infty}^{\infty}e^{ik_2y}\left[\int_{-\infty}^{\infty}e^{ik_1x}\,\bar{\eta}(k_1,k_2,t)\,dk_1\right]dk_2.$$
(33)

This inversion is computed by using the FFT. The inverse FFT is a fast algorithm for efficient implementation of the Inverse Discrete Fourier Transform (IDFT) given by

$$f(m,n)=\dfrac{1}{MN}\sum_{p=0}^{M-1}\sum_{q=0}^{N-1}F(p,q)e^{i\left(\frac{2\pi}{M}\right)pm}\,e^{i\left(\frac{2\pi}{N}\right)qn}\quad p=0,1,\ldots.,M-1,\ q=0,1,\ldots.,N-1,$$

where $f(m,n)$ is the resulted function of the two spatial variables $m$ and $n$, corresponding $x$ and $y$, from the frequency domain function $F(p,q)$ with frequency variables $p$ and $q$, corresponding $k_1$ and $k_2$. This inversion is done efficiently by using the Matlab FFT algorithm.

In order to implement the algorithm efficiently, singularities should be removed by finite limits as follows:

1. As $k \to 0$, implies $k_1 \to 0$, $k_2 \to 0$ and $\omega \to 0$ then $\overline{\eta}(k_1, k_2, t)$ has the limit

$$\lim_{k\to 0} \overline{\eta}(k_1, k_2, t) = 0 \text{ for } t \le t_1, \text{ where } t_1 = \frac{50}{v}.$$

2. As $k_1 \to 0$, then the singular term of $\overline{\eta}(k_1, k_2, t)$ has the following limits

$$\lim_{k_1 \to 0}\left(\frac{e^{-i\,200\,k_1} - e^{-i\,300\,k_1}}{i k_1}\right) = 100 \text{ and } \lim_{k_1 \to 0}\left(\frac{e^{i\,50\,k_1} - e^{-i\,50\,k_1}}{i k_1}\right) = 100.$$

3. As $k_2 \to 0$, then the singular terms of $\overline{\eta}(k_1, k_2, t)$ have the following limits

$$\lim_{k_2\to 0}\left(\frac{e^{-i\,150\,k_2}}{i k_2} - \frac{e^{i\,50\,k_2}}{i k_2}\right) = 100, \lim_{k_2\to 0}\left(\frac{4\sin(50k_2)}{k_2}\right) = 200,$$

$$\text{and } \lim_{k_2\to 0}\left(\frac{e^{-i\,50\,k_2}}{i k_2} - \frac{e^{-i\,150\,k_2}}{i k_2}\right) = 100.$$

Using the same steps, $\overline{\eta}(k_1, k_2, t)$ is evaluated by applying the Laplace and Fourier transforms to the bed motion described by (23) and (24), then substituting into (20) and then inverting $\overline{\eta}(k_1, k_2, s)$ using the inverse Laplace transform to obtain $\overline{\eta}(k_1, k_2, t)$. This is verified for $t_1 \le t \le t^*$ where $t^* = \frac{200}{v}$ as follows:

$$\overline{\eta}(k_1, k_2, t) = \overline{\eta}_{down}(k_1, k_2, t) + \overline{\eta}_{up}(k_1, k_2, t), \tag{34}$$

where

$$\overline{\eta}_{down}(k_1, k_2, t) = \overline{\eta}_{1down}(k_1, k_2, t) + \overline{\eta}_{2down}(k_1, k_2, t) + \overline{\eta}_{3down}(k_1, k_2, t),$$

hence,

$$\overline{\eta}_{down}(k_1, k_2, t) =$$

$$\begin{bmatrix} \left[\frac{-\zeta_0}{4\cosh(kH)}\right]\left[\frac{e^{i\,150\,k_2} - e^{i\,50\,k_2}}{i k_2} - \frac{1}{1-\left(\frac{100}{\pi}k_2\right)^2}\left[ik_2\left(\frac{100}{\pi}\right)^2(e^{i50k_2} + e^{i150k_2})\right]\right] + \\ \left[\frac{-\zeta_0}{\cosh(kh)}\right]\left[\frac{\sin(50k_2)}{k_2}\right] + \\ \left[\frac{-\zeta_0}{4\cosh(kH)}\right]\left[\frac{e^{-i\,50\,k_2} - e^{-i\,150\,k_2}}{i k_2} + \frac{1}{1-\left(\frac{100}{\pi}k_2\right)^2}\left[ik_2\left(\frac{100}{\pi}\right)^2(e^{-i150k_2} + e^{-i50k_2})\right]\right] \end{bmatrix} \times$$

$$\begin{bmatrix} \left[\frac{e^{i\,50\,k_1} - 1}{ik_1} + \frac{e^{i\,50\,k_1}}{1-\left(\frac{50}{\pi}k_1\right)^2}\left[ik_1\left(\frac{50}{\pi}\right)^2\left(1 - e^{-i50k_1}\right)\right]\right]\cos\omega(t - t_1) + \\ \frac{2v}{\omega^2 - (k_1v)^2}\left(\omega\sin\omega(t - t_1) + ik_1v\cos\omega(t - t_1) - ik_1ve^{-ik_1(t-t_1)v}\right) + \\ \left[\frac{e^{-ik_1((t-t_1)v) - e^{-ik_1(50+(t-t_1)v)}}}{i k_1} + \frac{1}{1-\left(\frac{50}{\pi}k_1\right)^2}\left[ik_1\left(\frac{50}{\pi}\right)^2(e^{-ik_1(50+(t-t_1)v)} + e^{-ik_1(t-t_1)v})\right]\right]\cos\omega(t - t_1) \end{bmatrix},$$

and $\bar{\eta}_{up}(k_1, k_2, t) = \bar{\eta}_{1up}(k_1, k_2, t) + \bar{\eta}_{2up}(k_1, k_2, t) + \bar{\eta}_{3up}(k_1, k_2, t)$, then

$$\bar{\eta}_{up}(k_1, k_2, t) =$$

$$\left[\begin{array}{c} \left[\frac{\zeta_0}{4\cosh(kH)}\right]\left[\frac{e^{i\,150\,k_2} - e^{i\,50\,k_2}}{i\,k_2} - \frac{1}{1-\left(\frac{100}{\pi}k_2\right)^2}\left[ik_2\left(\frac{100}{\pi}\right)^2(e^{i50k_2} + e^{i150k_2})\right]\right] + \\ \left[\frac{\zeta_0}{\cosh(kh)}\right]\left[\frac{\sin(50k_2)}{k_2}\right] + \\ \left[\frac{\zeta_0}{4\cosh(kH)}\right]\left[\frac{e^{-i\,50\,k_2} - e^{-i\,150\,k_2}}{i\,k_2} + \frac{1}{1-\left(\frac{100}{\pi}k_2\right)^2}\left[ik_2\left(\frac{100}{\pi}\right)^2(e^{-i150k_2} + e^{-i50k_2})\right]\right] \end{array}\right] \times$$

$$\left[\begin{array}{c} \left[\frac{e^{-i\,200\,k_1} - e^{-i\,250\,k_1}}{ik_1} + \frac{1}{1-\left(\frac{50}{\pi}k_1\right)^2}\left[-ik_1\left(\frac{50}{\pi}\right)^2(e^{-i250k_1} + e^{-i200k_1})\right]\right]\cos\omega(t - t_1) + \\ \frac{2ve^{-i\,250\,k_1}}{\omega^2 - (k_1v)^2}\left(\omega\sin\omega(t - t_1) + ik_1v\cos\omega(t - t_1) - ik_1ve^{-ik_1(t-t_1)v}\right) + \\ \left[\begin{array}{c}\frac{e^{-i\,k_1(250+(t-t_1)v)} - e^{-i\,k_1(300+(t-t_1)v)}}{i\,k_1} + \\ \frac{1}{1-\left(\frac{50}{\pi}k_1\right)^2}\left[ik_1\left(\frac{50}{\pi}\right)^2(e^{-i\,k_1(300+(t-t_1)v)} + e^{-i\,k_1(250+(t-t_1)v)})\right]\end{array}\right]\cos\omega(t - t_1) \end{array}\right].$$

Substituting $\bar{\eta}_{down}(k_1, k_2, t)$ and $\bar{\eta}_{up}(k_1, k_2, t)$ into (34) gives $\bar{\eta}(k_1, k_2, t)$ for $t_1 \leq t \leq t^*$. For the case $t \geq t^*$, $\bar{\eta}(k_1, k_2, t)$ will have the same expression as (34) except the term resulting from the convolution theorem, i.e.

$$\int_{(t-t_1)-t^*}^{t}\cos\omega\tau e^{-ik_1((t-t_1)v-\tau)}\,d\tau =$$

$$\frac{1}{\omega^2 - (k_1v)^2}\left[\begin{array}{c}\omega\sin\omega(t - t_1) + ik_1v\cos\omega(t - t_1) \\ -e^{-ik_1vt^*}\left(\omega\sin\omega((t - t_1) - t^*) + ik_1v\cos\omega((t - t_1) - t^*)\right)\end{array}\right],$$

instead of

$$\int_{(t-t_1)}^{t}\cos\omega\tau e^{-ik_1(t-\tau)v}\,d\tau = \frac{1}{\omega^2 - (k_1v)^2}\left(\omega\sin\omega(t - t_1) + ik_1v\cos\omega(t - t_1) - ik_1ve^{-ik_1(t-t_1)v}\right).$$

Finally, $\eta(x, y, t)$ is computed using inverse FFT of $\bar{\eta}(k_1, k_2, t)$.

Again, the singular points should be remove to compute $\eta(x, y, t)$ efficiently

1. As $k \to 0$, then $\bar{\eta}(k_1, k_2, t)$ has the following limit

$$\lim_{k\to 0}\bar{\eta}(k_1, k_2, t) = \left\{\begin{array}{c} 0\ (t - t_1) \leq t^* \\ 0\ (t - t_1) \geq t^* \end{array}\right., \text{where } t^* = \frac{200}{v}.$$

2. As $k_1 \to 0$, then the singular terms of $\bar{\eta}(k_1, k_2, t)$ have the following limits

$$\lim_{k_1\to 0}\left(\frac{e^{i\,50\,k_1} - 1}{ik_1}\right) = 50\ ,\ \lim_{k_1\to 0}\left(\frac{e^{-i\,k_1((t-t_1)v)} - e^{-i\,k_1(50+(t-t_1)v)}}{i\,k_1}\right) = 50,$$

$$\lim_{k_1\to 0}\left(\frac{e^{-i\,200\,k_1} - e^{-i\,250\,k_1}}{ik_1}\right) = 50\ \text{and}\ \lim_{k_1\to 0}\left(\frac{e^{-i\,k_1(250+(t-t_1)v)} - e^{-i\,k_1(300+(t-t_1)v)}}{i\,k_1}\right) = 50.$$

3. As $k_2 \to 0$ , then the singular terms of $\bar{\eta}( k_1, k_2, t )$ have the following limits

$$\lim_{k_2 \to 0} \left( \frac{e^{i\, 150\, k_2}}{i\, k_2} - \frac{e^{i\, 50\, k_2}}{i\, k_2} \right) = 100 \, , \lim_{k_2 \to 0} \left( \frac{\sin( 50 k_2)}{k_2} \right) = 50 \text{ and}$$

$$\lim_{k_2 \to 0} \left( \frac{e^{-i\, 50\, k_2}}{i\, k_2} - \frac{e^{-i\, 150\, k_2}}{i\, k_2} \right) = 100 .$$

Finally, $\bar{\eta}_{\text{block slide}} (k_1, k_2, t)$ is evaluated by applying the Laplace and Fourier transforms to the block slide motion described by (29), then substituting into (20) and then inverting $\bar{\eta}_{\text{block slide}} (k_1, k_2, s)$ using the inverse Laplace transform to obtain $\bar{\eta}_{\text{block slide}} (k_1, k_2, t)$.

This is verified for $t^* \leq t_2 \leq t^* + (L'/v)$ and $t^* + (L'/v) \leq t_3 \leq t^* + (2L'/v)$ .

Then,

$$\bar{\eta}_{\text{block slide}} (k_1, k_2, t) = \bar{\eta}_1(k_1, k_2, t) + \bar{\eta}_2(k_1, k_2, t) + \bar{\eta}_3(k_1, k_2, t). \tag{35}$$

Then,

$$\bar{\eta}_{\text{block slide}} (k_1, k_2, t) =$$

$$\left[ \begin{array}{l} \left[ \left[ \frac{\zeta_0}{4\cosh(kH)} \right] \left[ \frac{e^{i\,150\,k_2} - e^{i\,50\,k_2}}{i\,k_2} - \frac{1}{1 - \left( \frac{100}{\pi} k_2 \right)^2} \left[ ik_2 \left( \frac{100}{\pi} \right)^2 (e^{i50k_2} + e^{i150k_2}) \right] \right] \right] + \\ \left[ \frac{\zeta_0}{\cosh(kh)} \right] \left[ \frac{\sin(50k_2)}{k_2} \right] + \\ \left[ \frac{\zeta_0}{4\cosh(kH)} \right] \left[ \frac{e^{-i\,50\,k_2} - e^{-i\,150\,k_2}}{i\,k_2} + \frac{1}{1 - \left( \frac{100}{\pi} k_2 \right)^2} \left[ ik_2 \left( \frac{100}{\pi} \right)^2 (e^{-i150k_2} + e^{-i50k_2}) \right] \right] \end{array} \right]$$

$$\times \left[ \begin{array}{l} \left[ \left[ \frac{e^{-i\,(200+S)\,k_1} - e^{-i\,(250+S\,)k_1}}{ik_1} + \frac{1}{1 - \left( \frac{50}{\pi} k_1 \right)^2} \left[ -ik_1 \left( \frac{50}{\pi} \right)^2 (e^{-i(250+S)k_1} + e^{-i(200+S)k_1}) \right] \right] \cos\omega(t_3\text{-}t^*) \\ + \frac{2v e^{-i\,(250+S)\,k_1}}{\omega^2 - (k_1 v)^2} \left( \begin{array}{l} \omega\sin\omega t_3 + ik_1 v\cos\omega t_3 - \\ e^{-ik_1 vt^*}(\omega\sin\omega[t_3\text{-}t^*] + \\ ik_1 v\cos\omega[t_3\text{-}t^*]) \end{array} \right) \\ + \left[ \frac{e^{-i\,k_1(250+S+L)} - e^{-i\,k_1(\,300+S+L)}}{i\,k_1} + \frac{1}{1 - \left( \frac{50}{\pi} k_1 \right)^2} \left[ ik_1 \left( \frac{50}{\pi} \right)^2 (e^{-i\,k_1(\,300+S+L)} + e^{-i\,k_1(\,250+S+L)}) \right] \right] \cos\omega(t_3\text{-}t^*) \end{array} \right] .$$

Finally, $\eta(x, y, t_2, t_3 )$ is computed using inverse FFT of $\bar{\eta}( k_1, k_2, t_2, t_3 )$ .

Again, the singular points should be remove to compute $\eta(x, y, t )$ efficiently

1. As $k \to 0$, then $\bar{\eta}( k_1, k_2, t )$ has the limit

$$\lim_{k \to 0} \bar{\eta}( k_1, k_2, t ) = 100 \, (100 + 2L)\zeta_0 \, ,$$

2. As $k_1 \to 0$, then the singular terms of $\bar{\eta}(k_1, k_2, t)$ have the following limits

$$\lim_{k_1 \to 0}\left(\frac{e^{-i(200+S)k_1} - e^{-i(250+S)k_1}}{ik_1}\right) = 50 \text{ and } \lim_{k_1 \to 0}\left(\frac{e^{-ik_1(250+S+L)} - e^{-ik_1(300+S+L)}}{ik_1}\right) = 50.$$

3. As $k_2 \to 0$, then the singular terms of $\bar{\eta}(k_1, k_2, t)$ have the following limits

$$\lim_{k_2 \to 0}\left(\frac{e^{i150k_2}}{ik_2} - \frac{e^{i50k_2}}{ik_2}\right) = 100, \lim_{k_2 \to 0}\left(\frac{\sin(50k_2)}{k_2}\right) = 50 \text{ and } \lim_{k_2 \to 0}\left(\frac{e^{-i50k_2}}{ik_2} - \frac{e^{-i150k_2}}{ik_2}\right) = 100.$$

We investigated mathematically the water wave motion in the near and far-field by considering a kinematic mechanism of the sea floor faulting represented in sequence by a down and uplift motion with time followed by unilateral spreading in x-direction, both with constant velocity v, then a deceleration movement of a block slide in the direction of propagation. Clearly, from the mathematical derivation done above, $\eta(x, y, t)$ depends continuously on the source $\zeta(x, y, t)$. Hence, from the mathematical point of view, this problem is said to be well-posed for modeling the physical processes of the tsunami wave.

# 3. Results and discussion

We are interested in illustrating the nature of the tsunami build up and propagation during and after the movement process of a variable curvilinear block shape sliding. In this chapter, three cases are studied. We first examine the generation process of tsunami waveform resulting from the unilateral spreading of the down and uplift slip faulting in the direction of propagation with constant velocity v. We assume the spreading velocity of the ocean floor up and down lift equal to the tsunami wave velocity $v_t = \sqrt{gH} = 0.14$ km/sec as the largest wave amplitude occurs when $v = v_t$ due to wave focusing.

## 3.1. Tsunami generation caused by submarine slump and slide - Evolution in time

We assume the waveform initiated by a rapid movement of the bed deformation of the down and uplift source shown in Figure 2. Figure 6 shows the tsunami generated waveforms during the second stage at time evolution $t = 0.4t^*, 0.6t^*, 0.8t^*, t^*$ at constant water depth $H = 2$ km. It is seen how the amplitude of the wave builds up progressively as $t$ increases where more water is lifted below the leading wave depending on its variation in time and the space in the source area. The wave will be focusing and the amplification may occur above the spreading edge of the slip. This amplification occurs above the source progressively as the source evolves by adding uplifted fluid to the fluid displaced previously by uplifts of preceding source segments. This explains why the amplification is larger for wider area of uplift source than for small source area. It can be seen that the tsunami waveform $\eta/\zeta_0$ has two large peaks of comparable amplitudes, one in the front of the block due to sliding of the block forward, and the other one behind the block due to spreading of the depletion zone.
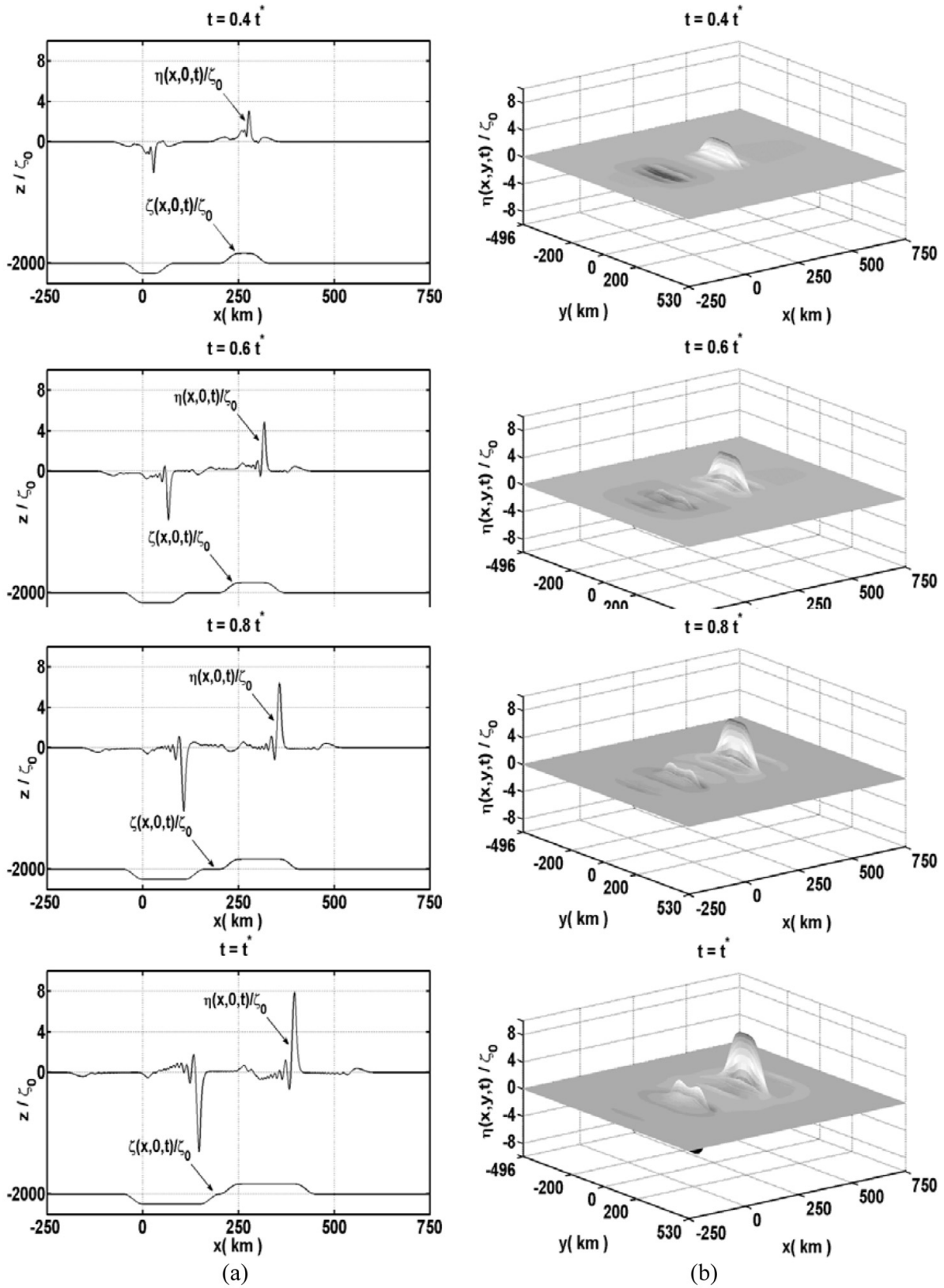
**Figure 6.** Dimensionless free-surface elevation caused by the propagation of the slump and slide in the x-direction during the second stage with $v = v_t$ at $H = 2$ km , $L = 150$ km, $W = 100$ km, $t^* = 200/v$ sec, (a) Side view along the axis of symmetry at $y = 0$ (b) Three dimensional view.

### 3.1.1. Effect of the water depth H

Figure 7 and Figure 8 illustrate the normalized peak tsunami amplitudes $\eta_{R,max}/\zeta_0$, $\eta_{L,min}/\zeta_0$ respectively in the near-field versus L/H at $t = t^* = t_1 + L/v$, the time when the spreading of the slides stops for H = 0.5, 1, 1.5 and 2 km and for $v = v_t$ and L = 150 km, W = 100 km.
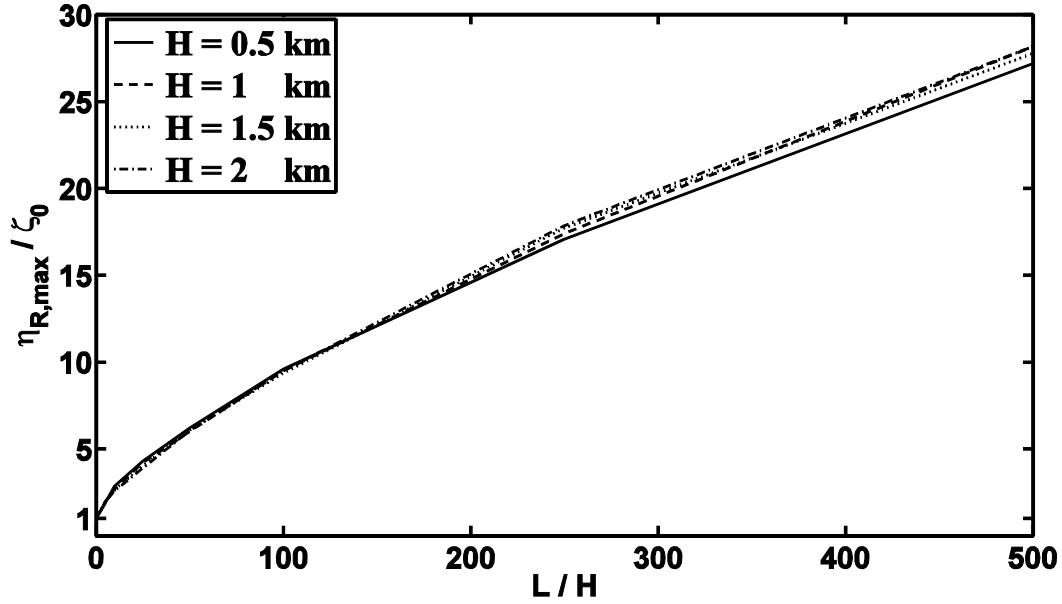


**Figure 7.** Normalized tsunami peak amplitudes, $\eta_{R,max}/\zeta_0$ at the end of second stage for different water depth H = 0.5, 1 , 1.5 and 2 km at $t^* = t_1 + L/v$ with $v = v_t$ and L = 150 km, W = 100 km.
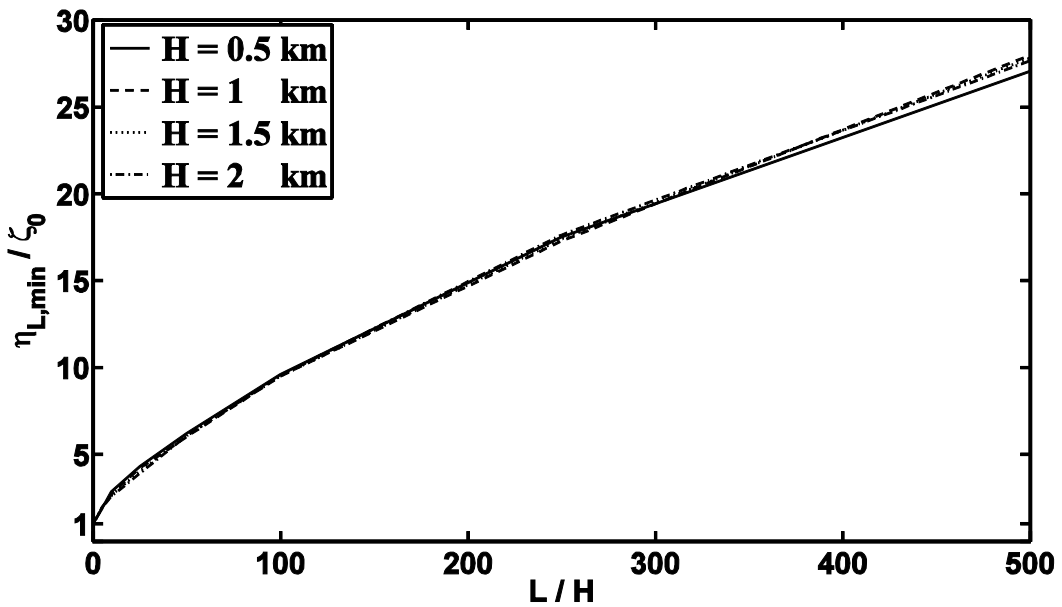


**Figure 8.** Normalized tsunami peak amplitudes, $\eta_{L,min}/\zeta_0$ at the end of second stage for different water depth H = 0.5, 1 , 1.5 and 2 km at $t^* = t_1 + L/v$ with $v = v_t$ and L = 150 km, W = 100 km.

From Figure 7 and Figure 8, the parameter that governs the amplification of the near-field water waves by focusing, is the ratio L/H. As the spreading length L in the slip-faults increases, the amplitude of the tsunami wave becomes higher.

At L = 0, no propagation occurs and the waveform takes initially the shape and amplitude of the curvilinear uplift fault (i.e. $\eta_{R,max}/\zeta_0 = 1, \eta_{L,min}/\zeta_0 = 1$).

The negative peak wave amplitudes are approximately equal to the positive peak amplitudes ($\eta_{L,min}/\zeta_0 \approx \eta_{R,max}/\zeta_0$) when $v = v_t$ as seen in Figures 7 and 8. The peak tsunami amplitude also depends on the water depth in the sense that even a small area source can generate large amplitude if the water is shallow.

### 3.1.2. Effect of the characteristic size

Figure 9 shows the effect of the water depth h on the amplification factor $\eta_{R,max}/\zeta_0$ for $v = v_t$, with $L = W = 10, 50, 100$ km and $L = 150$ km, $W = 100$ km at the end of the second stage (i.e. at $t = t^* = t_1 + L/v$). Normalized maximum tsunami amplitudes for 19 ocean depths are calculated. As seen from Figure 9, the amplification factor $\eta_{R,max}/\zeta_0$ decreases as the water depth H increases. This happens because the speed of the tsunami is related to the water depth ($v = v_t = \sqrt{gH}$) which produces small wavelength as the velocity decreases and hence the height of the wave grows as the change of total energy of the tsunami remains constant. Mathematically, wave energy is proportional to both the length of the wave and the height squared. Therefore, if the energy remains constant and the wavelength decreases, then the height must increases.
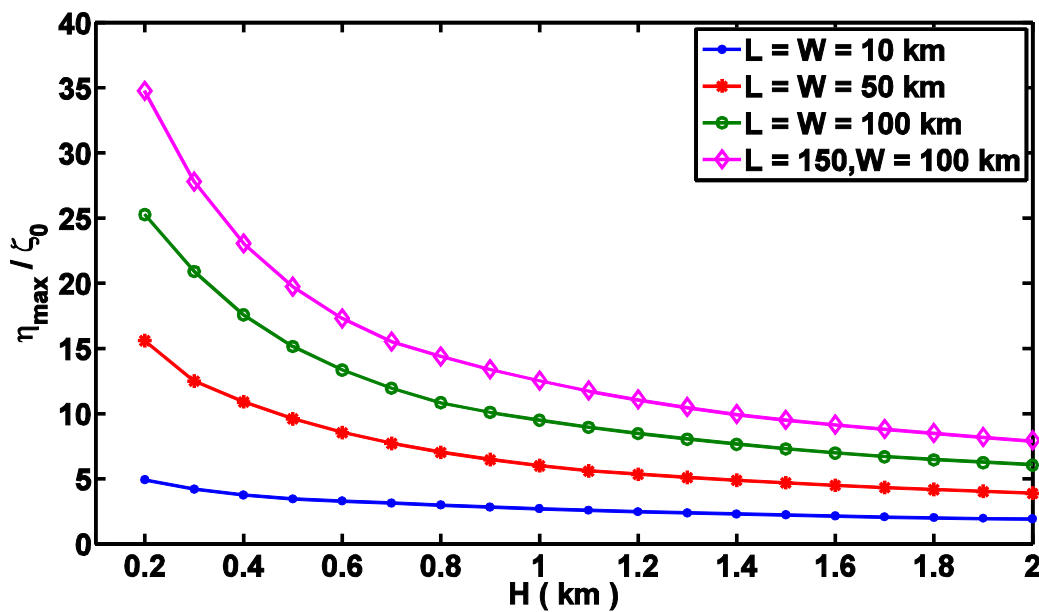


**Figure 9.** Normalized maximum tsunami amplitudes $\eta_{R,max}/\zeta_0$ for different length and width at $t = t^* = t_1 + L/v$ for $v = v_t$.

## 3.2. Tsunami generation and propagation-effect of variable velocities of submarine block slide

In this section, we investigated the motion of a submarine block slide, with variable velocities, and its effect on the near-field tsunami amplitudes. We considered the limiting case, in which the slide moves with constant velocity and stops suddenly (infinite deceleration) and the case in which the slide stops softly with constant deceleration for L = 150 km, W = 100 km and $v = v_t$.

### 3.2.1. Displaced block sliding with constant velocity v

Constant velocity implies that the slide starts and stops impulsively, i.e. the acceleration and deceleration are infinite both initially and finally. This means that the slide takes minimum time to reach the characteristic length $L' = 150$ km given by $t_{min} = t^* + (L'/v) = 41.65$ min. We illustrate the impulsive tsunami waves caused by sudden stop of the slide at distance $L'$ in Figure 10.
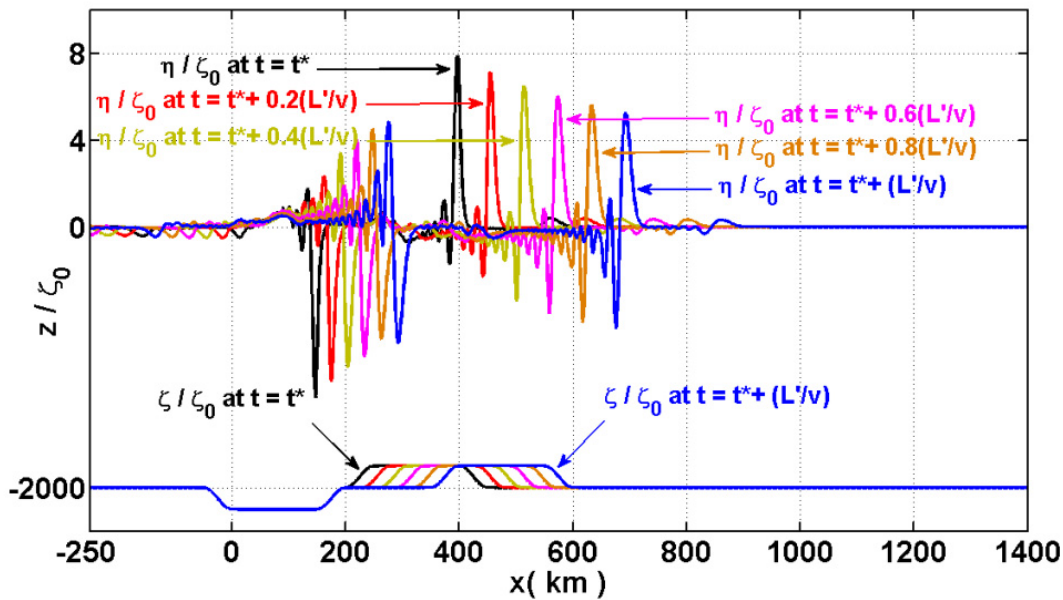


**Figure 10.** Normalized tsunami waveforms $\eta/\zeta_0$ along the axis of the symmetry at y = 0 and their corresponding moving slide $\zeta/\zeta_0$ with constant velocity v along y = 0, at time $t^* \leq t \leq t^* + (L'/v)$ for h = 2 km, $L' = 150$ km and W = 100 km.

Figure 10 shows the leading tsunami wave propagating in the positive x-direction during time evolution $t = t^*, t^* + 0.2(L'/v), t^* + 0.4(L'/v), t^* + 0.6(L'/v), t^* + 0.8(L'/v), t^* + (L'/v)$ sec at $L_E = 0, 30, 60, 90, 120, 150$ km respectively, where $L_E$ represents that part of L (see Figure 4c) for $v = v_t = 0.14$ km/sec. It is seen in Figure 10 that the maximum leading wave amplitude decreases with time, due to the geometric spreading and also due to the dispersion. At $t = t_{min} = t^* + (L'/v) = 41.65$, the wave front is at x = 693 km and $\eta_{R,max}/\zeta_0$ decreases from 7.906 at $t = t^*$ to 5.261 at time $t_{min}$. This happens because the amplification of the waveforms depends only on the volume of the displaced water by the moving source

which becomes an important factor in the modeling of the tsunami generation. This was clear from the singular points removed from the block slide model, where the finite limit of the free surface depends on the characteristic volume of the source model

### 3.2.2. Displaced block moving with linear decreasing velocity with time t

The velocity of the movable slide is uniform and equal $v(t)$ up to time $t_{max}$ as shown in Figure 4a, followed by a decelerating phase in which the velocity is given by

$$v(t) = v - (t - t^*)\alpha, \text{ for } t^* \leq t \leq t_{max}.$$

where $v = v_t = 0.14$ km/sec and $\alpha$ is the deceleration of the moving block slide. The block slide moves in the positive $x-$ direction with time $t^* \leq t \leq t_{max}$ where $t_{max} = t^* + 2L'/v$ is the maximum time that the slide takes to stop after reaching the characteristic length $L' = 150$ km with minimum deceleration $\alpha_{min}$. Figure 11 shows the leading tsunami wave propagating in the positive x-direction during time evolution $t = t^*, t^* + 0.2(2L'/v)$, $t^* + 0.4(2L'/v)$, $t^* + +0.6(2L'/v)$, $t^* + 0.8(2L'/v)$, $t^* + (2L'/v)$ min in case $t_2 = t^*$ (i.e. minimum magnitude of $\alpha$ ).
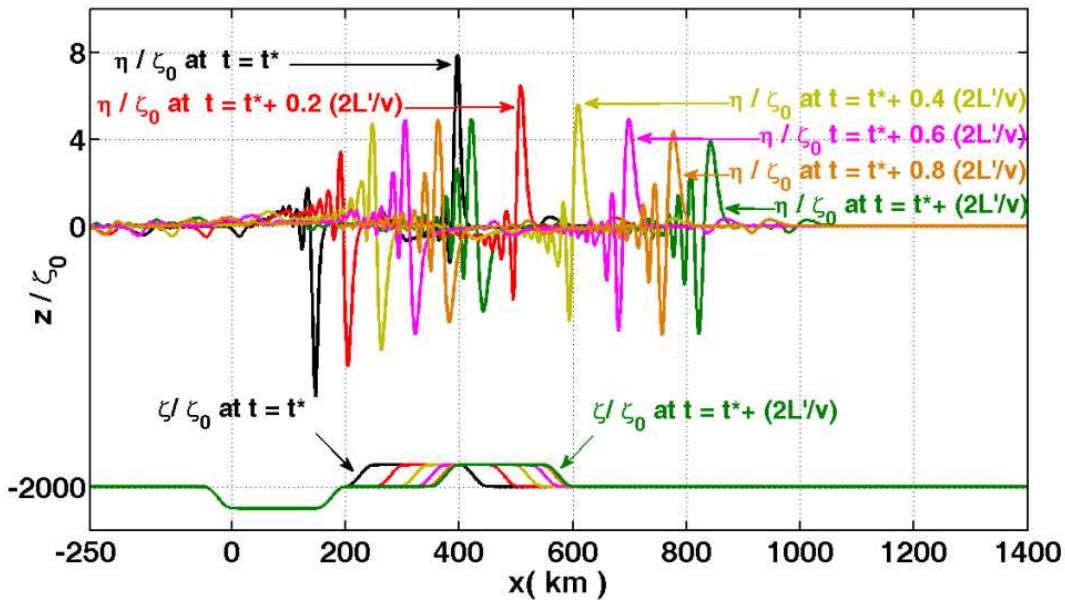


**Figure 11.** Normalized tsunami waveforms $\eta/\zeta_0$ and their corresponding moving slide $\zeta/\zeta_0$ with variable velocity $v(t)$ along $y = 0$, at time $t^* \leq t \leq t^* + 2L'/v$ at $H = 2$ km, $L' = 150$ km and $W = 100$ km.

It was clear from Figure 10 and Figure 11 that at the instant the slide stops, the peak amplitude in case of sudden stop is higher than that of soft stop.

Figure 12 and Figure 13 show the effect of the water depth at $L' = W = 10, 50, 100$ km and $L' = 150$, $W = 100$ km on the normalized peak tsunami amplitude $\eta_{R,max}/\zeta_0$ when the slide stops moving at length $L'$ instantaneously at $t_{min} = t^* + L'/v$ with infinite deceleration and stops moving softly at $L'$ at the time $t_{max} = t^* + 2L'/v$ with minimum deceleration for $v = v_t$.
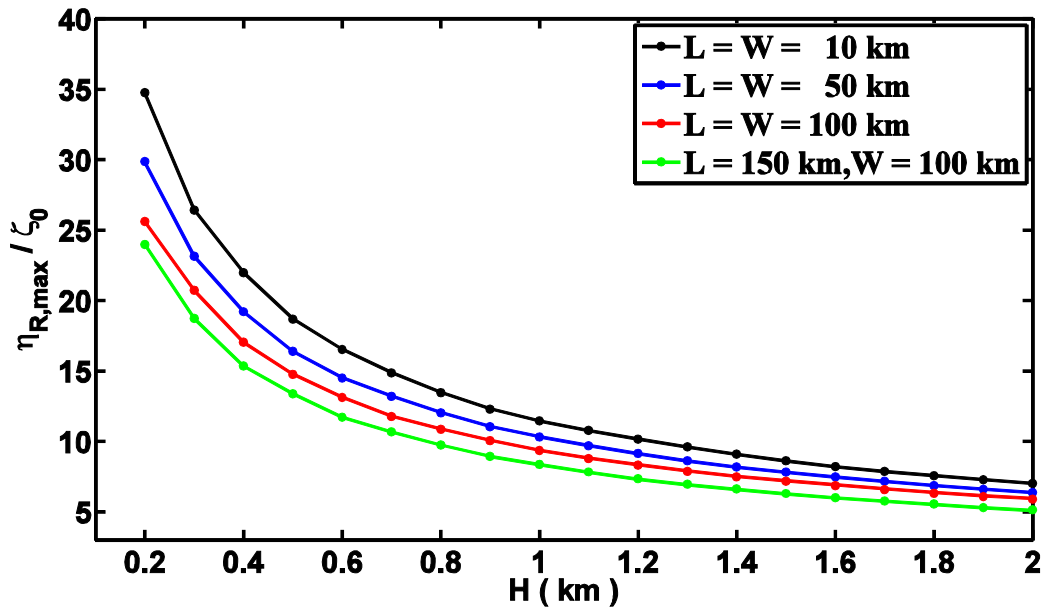
**Figure 12.** Normalized maximum tsunami amplitudes $\eta_{R,max}/\zeta_0$ when the slide stops suddenly at time $t_{min} = t^* + (L'/v)$ with different slide length L and width W and for $v = v_t$.
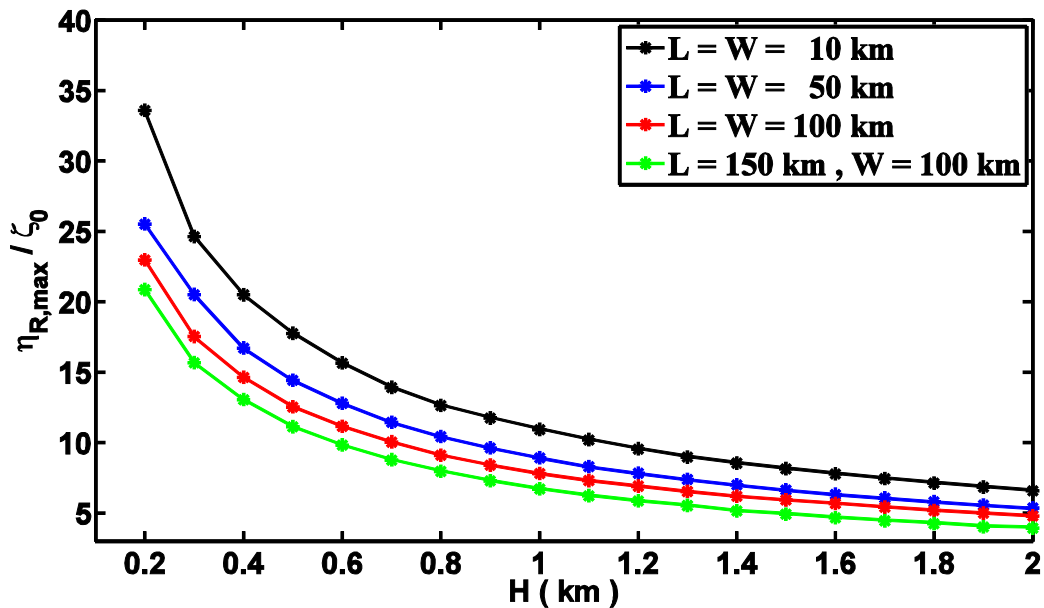


**Figure 13.** Normalized maximum tsunami amplitudes $\eta_{R,max}/\zeta_0$ when the slide stops softly at time $t_{max} = t^* + (2L'/v)$ with different slide length L and width W and for $v = v_t$.

It is clear from Figure 12 and Figure 13 that the waveforms which caused by sudden stop of the slide motion after they reach the characteristic length L′ at time $t_{min} = t^* + (L'/v)$ have higher amplitude than stopping of the slide with slow motion at time $t_{max} = t^* + (2L'/v)$ .This agrees with the mathematical relation between the wavelength and the wave height where the wave energy is proportional to both the length of the wave and the height squared.

### 3.2.3. Displaced block moving with constant velocity v followed by variable velocity $v(t)$

In this section, we studied the generation of the tsunami waveforms when the block moves a significant distance with constant velocity $v = v_t$ then continue moving with variable velocity v(t) with constant deceleration until it stops at the characteristic length $L' = 150$ km. Figure 14 shows the tsunami waveforms at the times calculated in Table 2 when the slide reaches the characteristic length $L' = 150$ km.
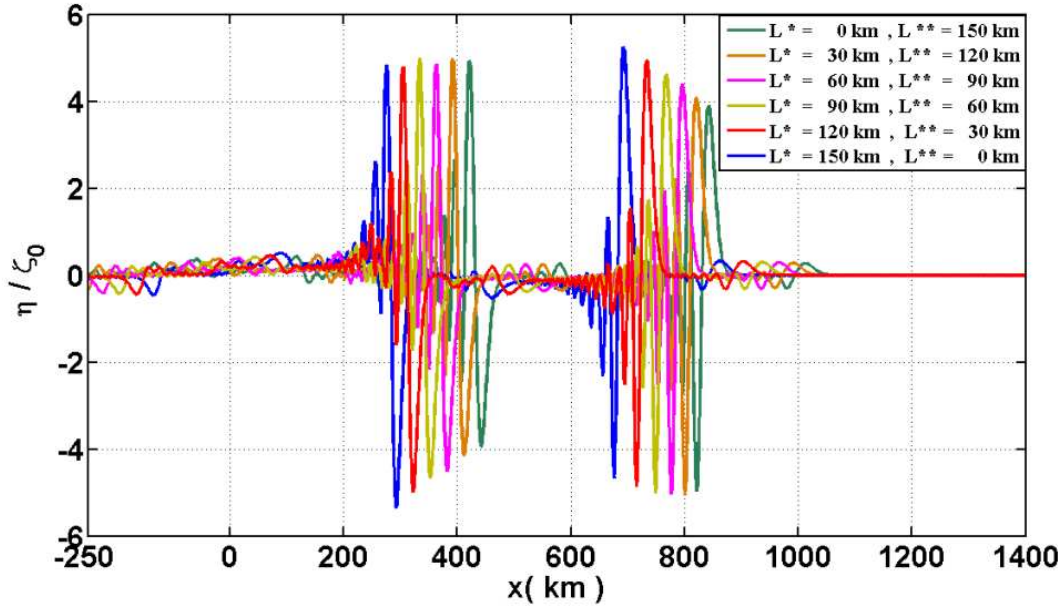


**Figure 14.** Normalized tsunami waveforms $\eta/\zeta_0$ along y = 0 at t = $t_3$ calculated in Table 7.2 with $L' = 150$ km.
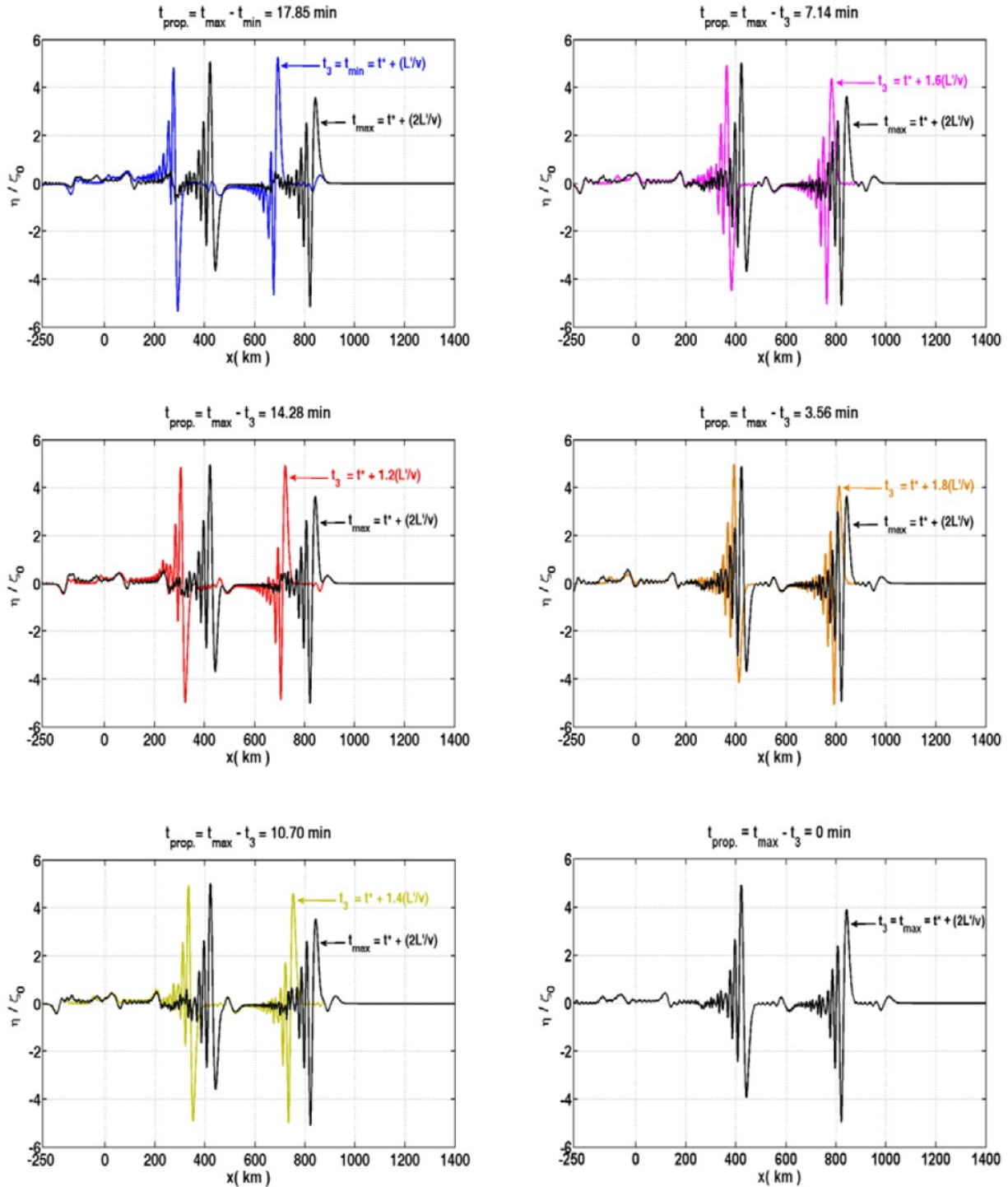
In Figure 14, the first waveform from the left indicates the shape of the wave at the time $t_3 = t_{min} = t^* + (L'/v) = 41.65$ in the limiting case when the slide stops moving suddenly. The last waveform indicates the wave in the other limiting case at the time $t_3 = t_{max} = t^* + (2L'/v)$ when the slide stop moving with minimum deceleration at the distance $L'$. In between the two limiting cases, the slide begins moving with constant velocity a significant distance followed by a decelerating movement until it stop at the characteristic length $L' = 150$ km at the time $t_{min} \leq t_3 \leq t_{max}$ , see Table 2. It is seen how the peak amplitudes of the leading waves decreases gradually from 5.261 to 3.894.

## 3.3. Tsunami propagation waveforms

In order to compare shape and maximum height of tsunami wave at certain time for different deceleration $\alpha$, we choose the time $t = t_{max}$. We study the case when the propagating waveforms resulting at the time difference between $t_3$ and $t_{max}$ (i.e. propagating of tsunami away from the slide) when the slide stops moving at the length $L'$.

For the limiting case $\alpha_{min}$, there is no free propagation, while for the other limiting case " the sudden stop", there is free propagation between time $t_{min}$ and $t_{max}$. For the cases between the two limiting cases, the propagation time is $t_{prop} = t_{max} - t_3$.

Figure 15 shows the shape of the tsunami propagation waveform at $t_{max} = t^* + (2L'/v) = 59.51$ min (curves in black) for different deceleration α and time $t_3$ (time at which the slide stops).



**Figure 15.** Normalized tsunami propagation waveforms η/ζ$_0$ along the axis of the symmetry at y = 0 at $t_{prop.} = 0, 3.56, 7.14, 10.70, 14.28, 17.85$ min with L' = 150 km and W = 100 km.

As the wave propagates, the wave height decreases and the slope of the front of the wave become smaller, causing a train of small wave forms behind the main wave. The maximum wave amplitude decreases with time, due to the geometric spreading and also due to the dispersion.

Figure 16 represents the normalized peak tsunami amplitudes $|\eta|_{min}/\zeta_0$ and $\eta_{max}/\zeta_0$ of the leading propagating wave in the far-field at time $t = t_{max}$ for the different deceleration $\alpha$ and time $t_3$ (time at which the slide stops) chosen in Figure 7.15.
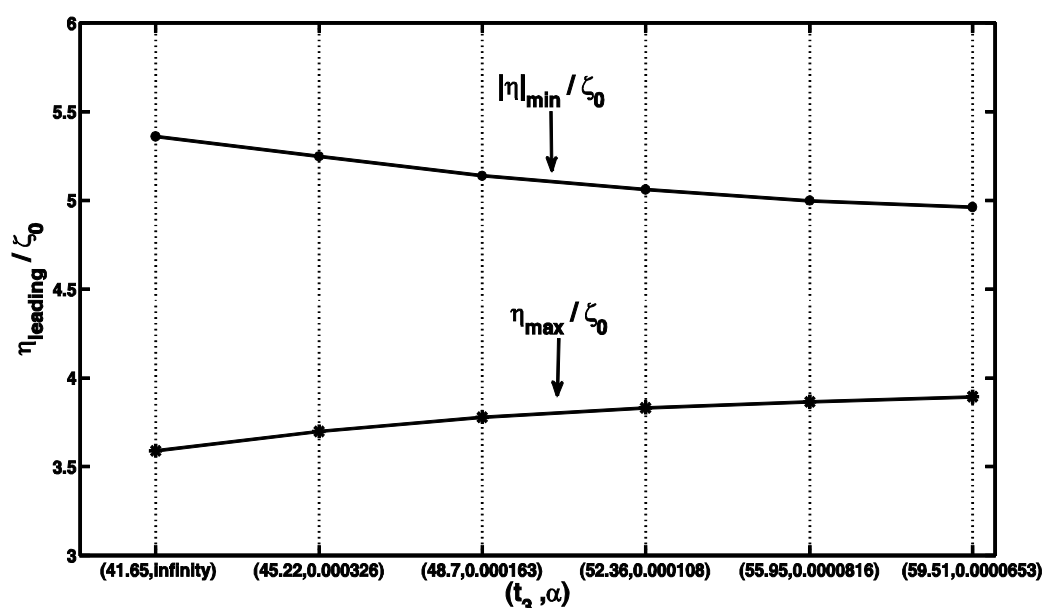


**Figure 16.** The normalized peak tsunami amplitudes $|\eta|_{min}/\zeta_0$ and $\eta_{max}/\zeta_0$ at time $t = t_{max}$ for the different deceleration $\alpha$ and time $t_3$.

It can be seen in Figure 16 that the absolute minimum peak amplitudes of the leading propagated waves at time $t_{max} = t^* + (2L'/v)$, after the block slide stops moving with different deceleration $\alpha$ and time $t_3$, decreases gradually, while the maximum peak amplitudes increases progressively.

## 4. Conclusion

In this paper, we presented a review of the main physical characteristics of the tsunami generation caused by realistic curvilinear submarine slumps and slides in the near-field. It is seen that the tsunami waveform has two large peaks of comparable amplitudes, one in the front of the block due to forward sliding of the block, and the other one behind the block due to spreading of the depletion zone. The negative peak wave amplitudes are approximately equal to the positive peak amplitudes. We studied the effect of variable

velocities of submarine block slide on the tsunami generation in the limiting cases, in which the slide moves with constant velocity and stops suddenly (with infinite deceleration) and the case in which the slide stops softly at the same place with minimum deceleration. It is seen that the leading tsunami amplitudes are reduced in both cases due to the geometric spreading and also due to the dispersion. We observed that the peak tsunami amplitudes increase with the decrease in the sliding source area and the water depth. We also investigated the more realistic case in which the block slide moves a significant distance with constant velocity $v$ then continue moving with time dependence velocity v(t) and different constant deceleration until it stops at the characteristic length. It is seen how the peak amplitudes of the leading waves decrease gradually with time between the two limiting cases. In this case we demonstrated also the shape of tsunami propagated wave at certain time max $t$ (time at which the slide stops with minimum deceleration). The results show that the wave height decreases due to dispersion and the slope of the front of the wave becomes smaller, causing a train of small wave forms behind the main wave. It can be observed that just a slight variation in the maximum and the minimum tsunami propagated amplitudes after the block slide stops moving with different deceleration α and time $t_3$, see **Figure 16**. The presented analysis suggests that some abnormally large tsunamis could be explained in part by variable speeds of submarine landslides. Our results should help to enable quantitative tsunami forecasts and warnings based on recoverable seismic data and to increase the possibilities for the use of tsunami data to study earthquakes, particularly historical events for which adequate seismic data do not exist.

## Author details

Khaled T. Ramadan
*Department of Basic and Applied Science, College of Engineering and Technology,*
*Arab Academy for Science, Technology and Maritime Transport, Abu Quir Campus, Alexandria,*
*Egypt*

## 5. References

[1] M. S. Abou-Dina and F. M. Hassan, "Generation and Propagation of Nonlinear Tsunamis in Shallow Water by a Moving Topography," *Applied Mathematics and Computation*, Vol. 177, No. 2, 2006, pp. 785-806.

[2] F. M. Hassan, "Boundary Integral Method Applied to the Propagation of Non-linear Gravity Waves Generated by a Moving Bottom," *Applied Mathematical Modelling*, Vol. 33, No. 1, 2009, pp. 451-466.

[3] N. Zahibo, E. Pelinovsky, T. Talipova , A. Kozelkov and A. Kurkin, "Analytical and Numerical Study of Nonlinear Effects at Tsunami Modeling," *Applied Mathematics and Computation*, Vol. 174, No. 2, 2006, pp. 795-809.

[4] Ben-Menahem and M. Rosenman, "Amplitude Patterns of Tsunami Waves from Submarine Earthquakes," *Journal of Geophysical Research*, Vol. 77, No. 17, 1972, pp. 3097-3128.

[5] Kjetil Braathen Haugen, Finn Løvholt and Carl B. Harbitz , " Fundamental mechanisms for tsunami generation by submarine mass flows in idealised geometries", Marine and Petroleum Geology, Vol. 22, Issues 1–2, 2005, pp 209–217.